Aus der

Klinik für Allgemeine, Viszerale und Transplantationschirurgie

Klinikum der Ludwig–Maximilians–Universität München

Direktor: Prof. Dr. med. Jens Werner

Role of VDR in stellate cells activation and tumor-stroma crosstalk in pancreatic cancer

Dissertation

zum Erwerb des Doktorgrades der Medizin

an der Medizinischen Fakultät der

Ludwig-Maximilians-Universität zu München

vorgelegt von

Yang Wu

aus Jiangsu, Volksrepublik China

2021

Mit Genehmigung der Medizinischen Fakultät

der Universität München

Berichterstatter:	Prof. Dr. med. Jens Werner
Mitberichterstatter:	PD Dr. med. Gerhard Preissler
	apl. Prof. Dr. med. Stefan Böck
Mitbetreuung durch den promovierten Mitarbeiter:	PD Dr. med. Jan G. D'Haese
Dekan:	Prof. Dr. med. dent. Reinhard Hickel
Tag der mündlichen Prüfung:	25.02.2021

LMU LUDWIG-MAXIMILIANS-UNIVERSITÄT MÜNCHEN

Dean's Office
Medical Faculty

MMRS

Affidavit

Wu, Yang

Surname, first name

Street

Zip code, town

Germany

Country

I hereby declare, that the submitted thesis entitled

Role of VDR in stellate cells activation and tumor-stroma crosstalk in pancreatic cancer

is my own work. I have only used the sources indicated and have not made unauthorized use of services of a third party. Where the work of others has been quoted or reproduced, the source is always given.

I further declare that the submitted thesis or parts thereof have not been presented as part of an examination degree to any other university.

Munich, 15/03/2021 Wu,Yang

Place, date Signature doctoral candidate

I. Table of Contents

I. Table of Contents 1

II. Abbreviation List 6

1. Introduction 10

1.1. Epidemiology of PDAC 10

1.2. PSCs in the tumor microenvironment (TME) of PDAC 12

1.2.1. Brief introduction of PSCs 12

1.2.2. PSCs enhance ECM secretion and reprogram TME in PDAC 14

1.2.3. PSCs increase chemoresistance in PDAC 14

1.2.4. PSCs enhance metastasis in PDAC 15

1.2.5. PSCs facilitate immune tolerance in PDAC 15

1.3. Current progress in PSCs-targeting strategies 15

1.3.1. Targeting tumor-originated sonic hedgehog (SHH) signaling pathway 16

1.3.2. Reprogramming strategies for PSCs 16

1.3.3. Strategies targeting stromal ECM production 17

1.4. Anti-fibrosis role of VDR and its ligands in diseases 21

1.4.1. VDR and its ligands in targeting myofibroblasts of non-cancer fibrotic diseases 21

1.4.2. VDR and its ligands in targeting cancer-associated fibroblasts (CAFs) 22

1.5. Objectives of this Project 23

2. Materials and Methods 24

2.1. Materials 24

2.1.1. Apparatus 24

2.1.2. Computer Software and Hardware 26

2.1.3. Experimental consumables 26

2.1.4. Chemical reagents and buffers 28

2.1.5. Kits and Primers 30

2.1.6. Antibodies 31

2.2. Methods 32

2.2.1. Primary PSCs Separation and Culture 32

2.2.2. PCCs Culture 37

2.2.3. Quantitative real-time polymerase chain reaction (qRT-PCR)..... 37

2.2.4. Proliferation Assay..... 39

2.2.5. Immunocytochemistry (ICC)..... 40

2.2.6. Wound Healing (WH) Test..... 40

2.2.7. Migration and Invasion Assessment..... 41

2.2.8. Western Blot (WB)..... 41

2.2.9. Statistical Analysis..... 48

3. Results..... 49

3.1. Establishment, verification of isolation of both activated and quiescent PSCs 49

3.1.1 Establishment of PSCs isolation..... 49

3.1.2 PSCs verification..... 53

3.2. Expression of VDR is higher in caPSCs than PCCs..... 54

3.3. VDR induction by its ligand decreases the PSCs activation..... 56

3.3.1. Vitamin D analog reduces αSMA expression in PSCs..... 56

3.3.2. Vitamin D analog decreases migration ability of activated PSCs..... 61

3.3.3. Vitamin D analog decreases proliferation ability of activated PSCs . 64

3.4. VDR activation in caPSCs attenuates caPSCs-augmented progression of PCCs 65

3.4.1. VDR activation in caPSCs decreases caPSCs-augmented migration ability of PCCs 65

3.4.2. VDR activation in caPSCs decreases caPSCs-augmented invasion ability of PCCs 67

3.4.3. VDR activation in caPSCs diminishes caPSCs-augmented proliferation ability of PCCs 69

4. Discussion 71

4.1. Isolation and verification of human PSCs 71

4.2. VDR in PSCs activation process 73

4.3. VDR in caPSCs-augmented aggressiveness of PCCs 75

4.4. Conclusion and Outlook 76

5. Summary 77

6. Zusammenfassung 78

III. Reference 80

IV. Acknowledgment 93

II. Abbreviation List

°C	Degree Celsius
%	Percentage
αSMA	α-smooth muscle actin
ASIR	Age-standardized incidence rates
APS	Ammonium persulfate
ATRA	All-trans retinoic acid
ASMR	Age-standardized mortality rates
AmB	Amphotericin B
Arc	Acrylamide
Ang-II	Angiotensin II
bFGF	Basic fibroblast growth factor
BSA	Bovine serum albumin
Cal	Calcipotriol
caPSCs	Cancer-associated PSCs
CP	Chronic pancreatitis
CRC	Colorectal cancer
CAFs	Cancer-associated fibroblasts
CT	Threshold cycle
CM	Conditioned medium
cpPSCs	Chronic pancreatitis-associated PSCs
CYP24A1	Cytochrome P450 family 24 subfamily A member 1
DIW	Deionized water

DMSO	Dimethyl sulfoxide
DCs	Dendritic cells
DAB	3,3’-diaminobenzidine
EMT	Epithelial-mesenchymal transition
ECM	Extracellular matrix
FBS	Fetal bovine serum
Gly	Glycine
GEM	Gemcitabine
GBSS	The Gey’s balanced salt solution
HA	Hyaluronidase
ICC	Immunocytochemistry
IL	Interleukin
h	Hour
HSCs	Hepatic stellate cells
HRP	Horseradish peroxidase
mL	Milliliter
min	Minutes
μm	Micrometer
mmol/L	Millimoles per liter
μL	Microliter
mAb	Monoclonal antibody
MMP	Matrix metalloproteinase
nm	Nanometer

nPSCs	Normal PSCs
OS	Overall survival
PCN	Penicillin
PDAC	Pancreatic ductal adenocarcinoma
PC	Pancreatic cancer
PBS	Phosphate-buffered saline
PCCs	Pancreatic cancer cells
PFS	Progression-free survival
PSCs	Pancreatic stellate cells
PDGF	Platelet-derived growth factor
qRT-PCR	Quantitative real-time polymerase chain reaction
s	Second
STR	Streptomycin
SHH	Sonic hedgehog
SDS	Sodium dodecyl sulfate
SDF-1	Stromal cell-derived factor 1
SSc	Systemic sclerosis
SD	Standard deviation
RT	Room temperature
TNF-α	Tumor necrosis factor-α
TME	Tumor microenvironment
TGF-β1	Transforming growth factor-β1
μg	Microgram

VDR	Vitamin D receptor
V	Volt
VEGF	Vascular endothelial growth factor
WH	Wound healing
WB	Western blot

1. Introduction

As a gastrointestinal malignancy with poor clinical outcomes[1], pancreatic cancer (PC) takes place when pancreatic cells grow out of control, develop into a lump and acquire the ability to invade other organs of the body[2, 3]. About 85% of PC is pancreatic ductal adenocarcinoma (PDAC)[4, 5]. The severe fibrogenic stroma reaction in PDAC enhances tumor progression and increases chemotherapy resistance[6-8]. Pancreatic stellate cells (PSCs), major producers of extracellular matrix (ECM), are known to participate in the stroma/desmoplasia reaction in PDAC and chronic pancreatitis (CP). Recently, targeting PSCs has emerged as a promising strategy for PDAC therapy[8, 9]. Many pieces of research have indicated that Vitamin D receptor (VDR) could reverse stroma fibrosis in many diseases, while little is known about its anti-PSCs effect in PDAC[10-14]. Therefore, this project is conducted to explore the role of a VDR ligand in the activation of PSCs and PSCs-augmented tumor progression in PDAC.

1.1. Epidemiology of PDAC

According to the estimates from GLOBOCAN 2018, PDAC ranks as the 11th most common carcinoma worldwide. Additionally, as the 7th primary cause of carcinoma mortality, PDAC caused 432,242 deaths in 2018[15]. The age-standardized incidence rates (ASIR) and morality rates (ASMR) differ significantly between regions, shown in Figure 1[15, 16]. Compared to women, the incidence of PDAC in men is slightly higher[15]. Despite increased awareness of the potential risk factors for PDAC and new early diagnostic tools, the incidence of PDAC is estimated to rise. According to the report of GLOBOCAN 2018, 355,317 new cases are expected to be diagnosed by 2040[15]. Until now, causes of PDAC are complex and not yet adequately recognized. However, several risk factors have been confirmed, for example, smoking, age, obesity, alcohol,

diabetes, family history, Helicobacter pylori infection, and CP [3, 17, 18]. The prognosis of PDAC is especially poor, as usually 24% of patients survive one year and 9% survive five years[4].

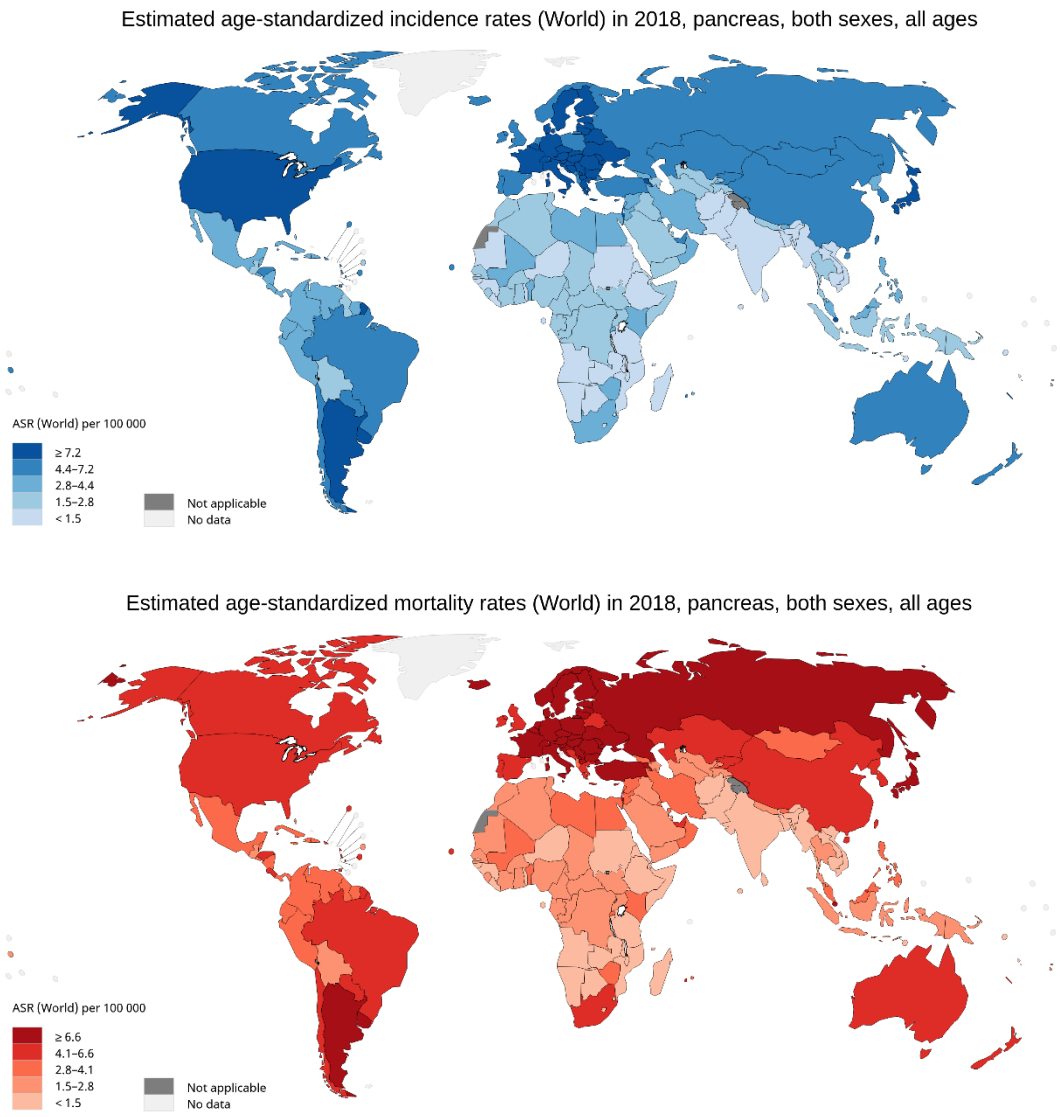

Figure 1: Maps indicate ASIR (up panel) and ASMR (low panel) for global PC in 2018 (from the website of Global Cancer Observatory: Cancer Today[16]).

1.2. PSCs in the tumor microenvironment (TME) of PDAC

The poor prognosis of PDAC is attributed to several reasons, among which the highly desmoplastic TME is the primary cause of treatment failure of conventional chemotherapy[19-21]. The TME, also known as the PDAC stroma, containing ECM, PSCs, endothelial cells, collapsed vessels, and immune cells, is reported to account for most PDAC volume[22, 23]. Constituting approximately 50% of the TME, PSCs have been considered one of the most prominent cell types of PDAC and have received great attention in recent decades[24-36].

1.2.1. Brief introduction of PSCs

About one century after Karl von Kupffer discovered hepatic stellate cells (HSCs) in 1876, similar star-shaped cells in the pancreas were found in 1982[37]. The in-vitro isolation and culture methods were not established until 1998[38, 39]. From then on, emerging research has focused on this new field, and PSCs are now well known as the leading cause of the stromal/desmoplasia reaction, which is the typical CP and PDAC[6, 40-42].

Located in peri-acinar or interlobular regions of the normal pancreas, PSCs are in quiescence, with many perinuclear droplets and low capacity to produce ECM[38, 39]. In diseases like PDAC or CP, quiescent PSCs get activated and change to a myofibroblast phenotype[43, 44]. Activated PSCs show positive immunostaining of α-smooth muscle actin (αSMA), no intracellular lipid droplets, enhanced release of numerous molecules, elevated migration and proliferation ability, and high ECM protein production[43, 44]. Figure 2 is a schematic diagram of the PSCs' activation procedure and PSCs-PCCs crosstalk. The following sections will focus on the main ways in which PSCs facilitate the progression of PDAC.

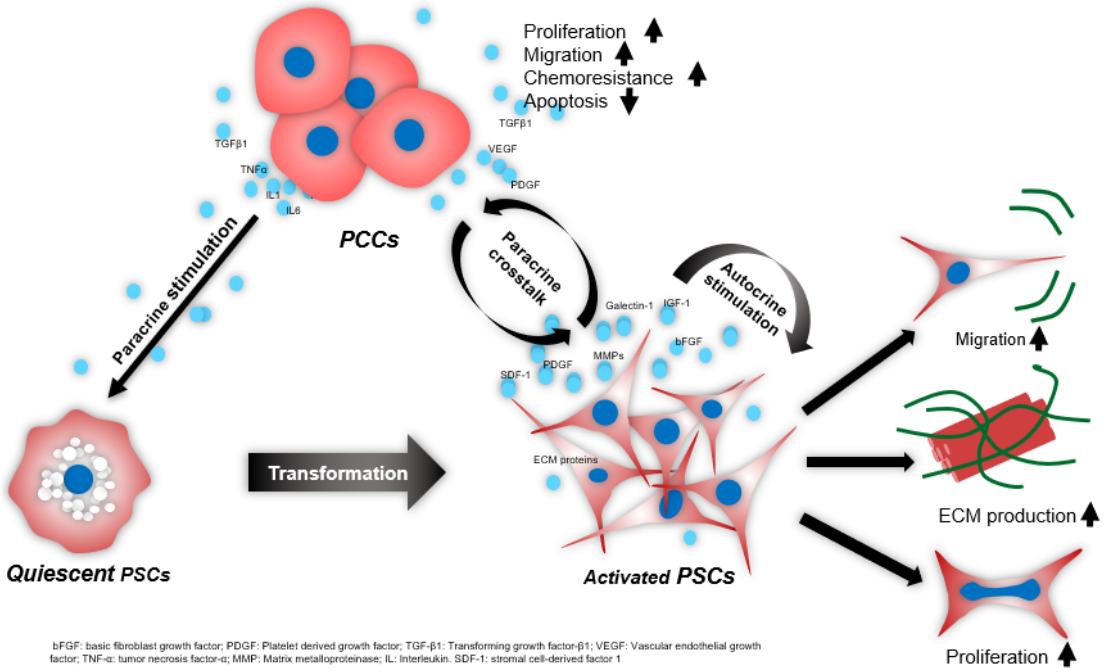

Figure 2: Schematic diagram of PSCs activation procedure and PSCs-PCCs crosstalk. PCCs induce PSCs transformation from quiescent to activated status by paracrine stimulation. Activated PSCs release various molecules, which in turn promote the aggressiveness of PCCs. In addition, PSCs remain activated, showing increased migration, proliferation, and ECM production via an autocrine way.

1.2.2. PSCs enhance ECM secretion and reprogram TME in PDAC

PSCs augment PDAC aggressiveness by causing chemoresistance via the severe stroma/desmoplasia reaction, which is attributed to the abundant ECM proteins secreted by PSCs[45]. This reaction also results in hypoxia in the tumor, epithelial-mesenchymal transition (EMT), enhanced malignant behavior of cancer, and chemoresistance[45]. PSCs were reported to improve the malignant behavior of PDAC by overproducing ECM proteins which regulate the phenotype of PDAC cells via the FAK/β1 integrin pathway[46].

The deposited ECM proteins form a dense barrier that inhibits chemotherapy drug delivery to PCCs via blood vessels[47]. The high ECM secretion also leads to increased pressure in pancreatic cancer[48], which contributes to vascular atrophy, insufficient blood flow, and depletion of nutrients[49]. Researches indicated that PSCs-PCCs crosstalk supported PDAC aggressiveness in the nutrient-depleted and hypoxic TME[50, 51]. Furthermore, exosomes secreted by PSCs are abundant in cellular metabolites like amino acids and palmitate, which fuel the tricarboxylic acid cycle in PDAC, thereby accelerating PDAC progression in the nutrient-depleted TME[52].

1.2.3. PSCs increase chemoresistance in PDAC

In addition to forming a physical barrier for chemotherapy drugs, PSCs increase chemoresistance by releasing numerous molecules, which play essential roles in the chemoresistance of PDAC cells[27, 49, 53]. For instance, periostin released by PSCs, keeping PSCs activated in an autocrine way, enhances the gemcitabine (GEM) resistance and invasion of PDAC cells via ERK1/2 and FAK/AKT pathway[54]. Furthermore, PSCs-secreted SDF-1α enhances resistance to GEM via ERK1/2 and FAK/AKT pathway in PDAC cells[55]. A recent study indicates that PSCs-derived fibronectin increases GEM chemoresistance in PDAC cells via the ERK1/2 pathway[56].

1.2.4. PSCs enhance metastasis in PDAC

The recent finding revealed that PSCs enhanced metastasis in PDAC by initiating EMT in PDAC cells[57]. Also, Schnittert et al. indicated that PSCs overexpressed integrin α11 and increased PSCs-augmented PDAC metastasis via paracrine TGF-β[58]. Researches also demonstrated that PSCs induced EMT, a well-known procedure of cancer metastasis initiation, in PDAC cells[57, 59]. Qian et al. revealed that galectin-1-overexpressed PSCs increased PDAC invasion and migration by secreting paracrine SDF-1 through the NFκB pathway[60].

1.2.5. PSCs facilitate immune tolerance in PDAC

Several studies indicated that PSCs significantly impacted immune tolerance in PDAC[61-64]. PSCs were reported to highly secret TGF-β1 and IL-10, which suppresses dendritic cells (DCs), thus impeding immune responses in PDAC[65]. Additionally, one study suggested that MDSCs might be stimulated to differentiate and expand by PSCs via IL-6/STAT-3 signaling and form a TME resistant to immunotherapy[49, 66]. Furthermore, PSCs reduced CD8+ T cells infiltration of the stromal juxtatumoral compartment, thereby hindering their access to PDAC cells[67].

1.3. Current progress in PSCs-targeting strategies

Although the field of PSCs is young, researchers have put up with several strategies to eliminate PSCs and reprogram TME by targeting PSCs or targeting the ECM production directly[26, 54, 60, 68-71]. A summary is shown in Table 1. The following parts will focus on current promising strategies.

1.3.1. Targeting tumor-originated sonic hedgehog (SHH) signaling pathway

PDAC cells are found to support stroma by the SHH pathway in a paracrine way[72]. An SHH inhibitor, IPI-926, combined with GEM could increase the vascular density and gemcitabine concentration in PDAC[72, 73]. However, an in-vivo study indicated that tumors from SHH-deleted PDAC mice showed a more invasive tumor behavior despite decreased stroma[74]. Therefore, the clinical trial of IPI-926 (phase II) was withdrawn because of increased mortality[75]. Similarly, in another in-vivo study, depletion of myofibroblasts in transgenic mice leads to more invasive and undifferentiated PDAC with reduced survival[76]. These works suggest that stroma functions are multifaced and simply deleting the whole stroma might result in the loss of fibrotic barriers that have an inhibitory function of metastasis. Therefore, current strategies have changed from simple stroma deletion to TME reprogramming or modulation with more beneficial outcomes[77-80].

1.3.2. Reprogramming strategies for PSCs

Many pieces of research have focused on reprogramming PSCs, reducing the activated state to reduce PSCs-augmented PDAC progression[79-81].

Previous studies indicated that Vitamin A analog was able to reprogram PSCs. For example, all-trans retinoic acid (ATRA) treated PSCs exhibited diminished activation, thereby leading to less behavior of PDAC cells[80, 82, 83]. Furthermore, an in-vivo study showed that PSCs were deactivated when treated by gold nanoparticles, which delivered ATRA plus heat-shock protein 47 siRNA, thereby improving GEM delivery to tumors in the mouse model of PDAC[84]. However, clinical trials on vitamin A analog showed disappointing outcomes. A pilot phase II trial in England indicated that drug combination (GEM plus 13-cis-RA) showed no improvement in the response rate of

unresectable PDAC[85]. Another Pilot phase II trial in the USA also showed that drug combination (13-cis-RA plus interferon-α) displayed no anti-tumor effects on PDAC[86].

Pirfenidone has been shown to reduce PSCs activation, collagen secretion, and periostin, thereby attenuating proliferation and metastasis in the PDAC mouse model[87]. Compared to treatment with GEM alone, pirfenidone plus GEM diminished tumor progression by deactivating PSCs[87]. In another PDAC research, pirfenidone plus N-acetyl cysteine decreased fibrotic reaction, cancer cell growth, and metastasis in a hamster model[88].

Attempts were also made in reprogramming PSCs by miRNAs, which is a potential therapeutic target[89]. miRNA-29 was found to be reduced in activation procedure PSCs in PDAC[90]. Restoring miRNA-29 expression in PSCs reduced desmoplasia reaction and PDAC aggressiveness[90]. A recent study indicated that miRNA let-7d impeded PSCs activation by targeting thrombospondin 1 and subsequently decreased pancreatic fibrosis[91].

Some other promising targets are also reported recently. The endogenous lipid Lipoxin A4 is demonstrated to impede the activation procedure of PSCs, which causes decreased tumor volume and aggressiveness in vivo[78]. Additionally, galectin-1 is upregulated in PSCs and correlated with dismal clinical outcomes of PDAC[60]. Galectin-1 deleted mice showed a reduced PSCs activation, enhanced T cell infiltration, and attenuated metastasis of tumor[92].

1.3.3. Strategies targeting stromal ECM production

As described in section 1.2.2., the high solid stress caused by PSCs-released ECM is closely correlated with chemoresistance. Therefore, several pieces of research have focused on the strategy of interstitial decompression[48, 62, 93].

GEM combined with PEGPH20, a drug based on the recombinant human hyaluronidase (HA) enzyme, was found to promote survival and reduce the malignant behavior of tumors in the PDAC mice model[93]. A Phase I trial also indicated promising outcomes that patients treated with PEGPH20 plus GEM showed prolonged overall and progression-free survival (OS and PFS) rates [94]. Moreover, the phase II trial drug combination (PEGPH20+nab-paclitaxel+GEM) showed increased PFS in patients with high-HA PDAC[95].

Angiotensin II (Ang-II) was found to promote proliferation and ECM production of PSCs[81]. Therefore, the angiotensin blockers are of the therapeutic potential, and two Ang-II type I receptor inhibitors were investigated. Olmesartan reduced collagen I production of PSCs and impeded tumor growth in the PDAC mouse model[96]. The other inhibitor, losartan, decreased pressure in tumors and increased vascular perfusion by reducing collagen and HA production in PSCs, which improved chemotherapy in PDAC mouse models[97].

Table1 Strategies targeting PSCs in TME of PDAC

Strategies	Main results
Clinical studies	
PEGPH20	Phase Ib: Elevated OS and PFS in PDAC patients[94].
IPI-926	Phase II: Withdrawn for enhanced mortality[75].

Marimastat	Phase II: No extra benefits were found in PDAC patients compared to GEM alone[98].
ATRA	Phase Ib: Ongoing, no results released[99].
Preclinical studies	
IPI-926	elevated vascular density and concentration of GEM in tumor of KPC mice[73].
Minnelide	reduced ECM production, increased vasculature, improved drug delivery in tumors in both spontaneous KPC mice and PDAC xenograft mice[100].
BET inhibitors	Attenuated PSCs activation and collagen I production in the mouse model of PDAC[101].
αSMA$^+$ cells deletion	Resulted in more aggressive tumors, increased hypoxia, EMT, and reduced survival in transgenic PDAC mice, which deleted αSMA$^+$ cells[76].
SHH deletion	Led to undifferentiated malignancies, increased vascularity, and proliferation in SHH-deleted PDAC mice[74].
PEGPH20	Depleted HA, expanded blood vessels, and increased chemotherapeutic drug delivery in tumors of PDAC mice[48].
Pirfenidone	Reduced PSCs proliferation, collagen production; co-treatment with GEM reduced tumor growth and hepatic metastasis in PDAC mice[88].
Olmesartan	Decreased PSCs proliferation, αSMA expression, collagen I production, tumor growth in subcutaneous PDAC mice[96].

Losartan	Decreased stress in solid tumors, improved vascular perfusion, increased chemotherapeutic delivery in PDAC mice[97].
ATRA	Decreased PSCs migration, collagen synthesis, leading to increased apoptosis of surrounding PSCs[80].
Calcipotriol	Improved intratumoral concentration of a chemotherapeutic drug, decreased tumor size, prolonged survival compared to GEM alone in KPC mice[79].
LXA4	Reduced PSCs activation, fibrosis, and tumor growth of in mice model[78].
Rho-associated protein kinase inhibitor	Reduced PSC activation, decreased collagen deposition, increased GEM delivery, improved OS in PDAC mice model[69].
AZ13381758	reduced collagen I/III, lowered metastasis, increased OS in the PDAC mice model[102].
peptidomimetic AV3	reduced desmoplasia, decompressed blood vasculature, improved GEM efficacy in patient-derived xenograft tumor models[29].
AMD3100	increased T cell infiltration, reduced tumor growth in PDAC mice model[103].

1.4. Anti-fibrosis role of VDR and its ligands in diseases

1.4.1. VDR and its ligands in targeting myofibroblasts of non-cancer fibrotic diseases

In several non-cancer fibrotic diseases, VDR and its ligands have been widely investigated. Several studies have demonstrated that VDR ligands mainly target myofibroblasts and impede the pro-fibrotic function of TGFβ[104-107]. For instance, in hepatic fibrosis, quiescent HSCs were activated by the TGFβ1/SMADs pathway and changed to an activated state, which produced abundant ECM proteins[108, 109]. In a study using carbon tetrachloride mouse model of hepatic fibrosis, treatment with VDR ligands deactivated HSCs and abolished hepatic fibrosis, while VDR-knockout led to spontaneously developed liver fibrosis[14]. As to the mechanism, TGFβ1 signaling redistributes the VDR-binding sites in HSCs[14]. VDR ligands induce VDR to bind to the SMAD3 pro-fibrotic genes, which reduces the binding of SMAD3 at these sites, thereby inhibiting fibrosis[14]. Similar results were found in another research indicating that rat HSCs treated with vitamin D (VD) show reduced fibrosis by impeding the promoter activity of collagen 1α[110]. In a study of systemic sclerosis (SSc), a disease with excessive accumulation of ECM contents, researchers showed that VDR induction by its ligand decreased the stimulating effects of TGFβ on fibroblasts differentiation into myofibroblast, thereby preventing collagen production and fibrosis in the SSc mouse model[111]. Besides, VDR ligand was shown to inhibit the TGFβ1-intermediated pro-fibrotic effect in human primary cardiac fibroblasts[112]. Furthermore, VDR ligand treatment prevented bleomycin-generated lung fibrosis in a mouse model of idiopathic pulmonary fibrosis by deactivating TGFβ1-induced SMAD3 phosphorylation[10].

1.4.2. VDR and its ligands in targeting cancer-associated fibroblasts (CAFs)

Unlike those in non-cancer diseases, not many studies about the relationship between VDR and CAFs are found, and it remains a new area to be studied. In colorectal cancer (CRC), investigations have demonstrated that VD diminished tumorigenesis in animal models of CRC[113], and VD deficiency is correlated with an elevated risk of CRC[114-116]. Higher VDR expression in CAFs was related to a longer OS in CRC patients, and VDR ligand showed a protective effect against CRC by reprogramming CAFs[117]. Sherman et al. showed that VDR ligand could decrease inflammation and enhanced the intratumoral concentration of GEM in the PDAC mouse model[79]. Moreover, Kong et al. demonstrated that VDR induction by its ligand in pancreatic CAFs inhibited exosomal miR-10a-5p secretion, an oncomiRNA, thus reducing its tumorigenic effects on PDAC cells[118]. However, detailed mechanisms by which VDR modulates CAFs and tumor-stroma crosstalk remained to be clarified.

Since fibrotic stroma is essential in tumor progression, the VDR-intermediated remodeling of stroma might be a promising therapeutic method to enhance conventional chemotherapy in PDAC and other stroma-abundant tumors.

1.5. Objectives of this Project

The general purpose of our project is to obtain a deeper understanding of VDR in PSCs activation and tumor-stroma crosstalk. For this purpose, the following questions are to be explored:

a). Establishment and verification of the isolation of both quiescent PSCs and activated PSCs.

b). How is the expression of VDR respectively in tumor cells and caPSCs isolated from human samples?

c). Can VDR induction by its ligand inhibit the activation of PSCs?

d). To what extent does the modulation of VDR in caPSCs influence the tumorigenic properties of PCCs?

2. Materials and Methods

2.1. Materials

2.1.1. Apparatus

Autoclave	Unisteri, Germany
BD LSRFortess™ cell analyzer	BD Bioscience, Germany
Centrifuge	Heraeus, Germany
Cell culture incubator	Binder, Germany
Combitips Plus	Sigma-Aldrich, US
Cool centrifuge	Eppendorf, Germany
CO_2 Incubator	Binder, Germany
CO_2 Incubator	Thermo Fisher Scientific, US
Micro centrifuge	Labtech, Germany
Microwave oven	Siemens, Germany
DNA workstation	Uni Equip, Germany
Drying cabinet	Heraeus, Germany
Electronic pH meter	Knick, Germany
Fluorescence Microscope	Zeiss, Germany
Hypercassette	Amersham Biosciences, Germany
Ice machine	KBS, Germany

Lamina flow	Hereaus flow laboratoies, Germany
Liquid nitrogen tank	MVE, US
Microscope	Olympus, Germany
Micro weigh	Chyo, Germany
Microplate reader	VERSA max, Germany
Mini electrophoretic transfer cell	Bio-Rad, Germany
Multipette Plus	Eppendorf, Germany
Nanodrop 2000	Thermo fisher scientific, US
Pipettes	Sigma-Aldrich, US
Pipette controller	Eppendorf, Germany
Power supply power pac 300	Bio-Rad, Germany
DNA workstation	Uni Equip, Germany
Shaker	Edmund Buehler, Germany
Step one PCR system	Applied Biosystems, Germany
Thermocycler	Eppendorf, Germany
Thermomixer comfort	Eppendorf, Germany
UV illuminator	Labortechnik, Germany
Vortex	Labnet, Germany
Water bath	Memmert, Germany
Water bath for shaking	Kottermann Labortechnik, Germany

X cell II TM Blot module	Invitrogen, Germany
Fridge (4°C, -20°C, -80°C)	Siemens, Germany

2.1.2. Computer Software and Hardware

Endnote X9	Clarivate Analytics, US
GraphPad Prism	Version 7.0, US
Image J	National Institutes of Health, US
SPSS	Version 21, US
Hardware	HP, US

2.1.3. Experimental consumables

Blot paper	Bio-Rad, Germany
Cell flasks (T25, T75, T125)	Thermo Fisher Scientific, Denmark
Cell scrapers	Sigma-Aldrich, Germany
Cell strainer (40µm, 70µm, 100µm)	BD Bioscience, US
Disposable safety scalpels #22	Thermo Fisher scientific, Germany
10µl T.I.P.S.	Eppendorf, Germany
20µl T.I.P.S.	Eppendorf, Germany
100µl T.I.P.S.	Eppendorf, Germany
200µl T.I.P.S.	Eppendorf, Germany

1mL T.I.P.S.	Eppendorf, Germany
Film ECL	GE healthcare, Germany
15mL Falcon tube	TPP, Switzerland
50mL Falcon tube	Corning, Mexico
Filters 0.25µm	Sartorius, Germany
Filters 0.45µm	Sartorius, Germany
Glass cover slips	Thermo Fisher Scientific, Germany
Green gloves	SHIELD Scientific, Netherlands
Glass slides	Thermo Fisher Scientific, Germany
Hydrophobic pen	Dako, Denmark
Immobilon-PSQ PVDF transfer membrane	Sigma-Aldrich, Germany
Orange gloves	SHIELD Scientific, Netherlands
Plates (6-, 12-, 24-, 96-well)	Thermo Fisher scientific, Denmark
5mL Pipette	Costar, US
10mL Pipette	Costar, US
25mL Pipette	Costar, US
50mL Pipette	Costar, US
Sterile needle	BD Bioscience, Spain

2.1.4. Chemical reagents and buffers

Amphotericin B (AmB) solution	Sigma-Aldrich, DE
Ammonium persulfate (APS)	Serva, US
Bovine Serum Albumin(BSA)	Biomol,DE
β-Mercaptoethanol	Sigma-Aldrich, DE
Collagenase P	Roche, DE
Crystal violet	Sigma-Aldrich, DE
$CaCl_2 \cdot 2H_2O$	Merck, DE
Calcipotriol (Cal)	Sigma-Aldrich, DE
Dimethyl sulfoxide (DMSO)	Sigma-Aldrich, DE
DNase	Roche, DE
Dulbecco's modified Eagle medium (DMEM)	Gibco, US
D-(+)-Glucose	Sigma-Aldrich, DE
DMEM/F12	Gibco, US
EDTA	Calbiochem, DE
ECL™ Western blotting system	Amersham Biosciences, DE
70% Ethanol	Apotheke GH, DE
96% Ethanol	Apotheke GH, DE
>99% Ethanol	Apotheke GH, DE
FBS	Sigma-Aldrich, DE

Glycine (Gly)	Roth, DE
IC Fixation buffer	Thermo Fisher Scientific, DE
Isopropanol	Roth, DE
KCl	Serva, DE
KH_2PO_4	Sigma-Aldrich, DE
Loading buffer 4X	Bio-Rad, USA
Methyl cellulose	Sigma-Aldrich, DE
$MgCl_2 \cdot 6H_2O$	Fluka, Switzerland
$MgSO_4 \cdot 7H_2O$	Merck, DE
Milk powder	Roth, DE
$NaHCO_4 \cdot 2H_2O$	Merck, DE
NaCl	Sigma-Aldrich, DE
Nycodenz	Axis-shield PoC, Norway
$NaHCO_3$	Sigma-Aldrich, DE
phosphate-buffered saline (PBS)	PAN-Biotech, DE
Penicillin-Streptomycin (PCN-STR) Mixture	Lonza, US
Permeabilization Buffer 10X	Thermo Fisher Scientific, DE
4% PFA	Pharmcy, DE
37% PFA	Applichem, DE
30% Acrylamide (Arc)	Roth, DE

Pronase	Roche, DE
Protease from stretomyces griseus	Sigma-Aldrich, US
Standard proteins	Bio-Rad, US
Protease inhibitor cocktail	Roche, DE
RPMI 1640	Gibco, US
RNase-free water	Qiagen, DE
RIPA lysis buffer 10X	Millipore, DE
Sodium dodecyl sulfate (SDS)	Roth, DE
Trypan blue	Sigma-Aldrich, DE
TEMED	Bio-Rad, US
Triton-X-100.	Sigma-Aldrich, Switzerland
Trypsin EDTA	Lonza, Switzerland
Tris base	Bio-Rad, US
Tween 20	Sigma-Aldrich, DE
Verse Solution	Gibco, US

2.1.5. Kits and Primers

BCA protein kit	Thermo Fisher Scientific, DE
EZ4U	Biomedica, Austria

cDNA Synthesis kit	Bio-Rad, US
ImmPACT DAB Peroxidase substrate kit	VECTOR, DE
Matrixgel Matrix	Corning, DE
QuantiTect Reverse Transcription Kit	Qiagen, DE
QuantiTect Primer Assay (200)	Qiagen, DE
RNeasy Micro Kit	Qiagen, DE
Sso Fast Eva Green	Bio-Rad, DE
Polyester Membrane Cell Culture Inserts	Corning, DE
ACTB	Qiagen, DE
αSMA	Qiagen, DE
Cytochrome P450 family 24 subfamily A member 1 (CYP24A1)	Qiagen, DE
GAPDH	Qiagen, DE
VDR	Qiagen, DE

2.1.6. Antibodies

Antibody	**Source**
Horseradish peroxidase (HRP)-linked anti-rabbit IgG	Cell signaling Technology (CST), DE
Vitamin D3 (D2K6W) receptor Rabbit monoclonal antibody (mAb)	CST, DE

α-Smooth muscle actin Ab	CST, DE
GAPDH antibody (FL-335)	Santa Cruz Biotechnology, DE
GAPDH (D16H11) XP Rabbit mAb	CST, DE
IRDye (800CW, 680RD) goat anti-rabbit Ab	LI-COR, US
Anti-human Desmin Clone D33 Mouse mAb	Dako, Denmark
HRP-conjugated goat anti-mouse IgG	Santa Cruz Biotechnology, DE
Anti-human smooth muscle actin clone 1A4 mouse mAb	Dako, Denmark

2.2. Methods

2.2.1. Primary PSCs Separation and Culture

Activated PSCs were separated employing the outgrowth method[39], employing surgically resected pancreas tissues from patients with PDAC or CP. Briefly, after removing the adipose and connective sections, tissue blocks were sliced into tiny fragments (0.5-1mm^3) with scalpels and were grown in six-well plates (5-10 pieces/well). A complete fresh medium containing 20% FBS (Table 2) was added. The tissue pieces were then kept in the incubator (37°C, humidified atmosphere, 5% CO_2/air), and the medium was refreshed after one day. PSCs emerged from tissue blocks 3-5 days later, and tissue fragments were eliminated as PSCs reached a 20% confluence, and the medium was renewed twice every week. PSCs were harvested and cryopreserved in liquid nitrogen when they were 80% confluent.

Human quiescent pancreatic stellate cells (PSCs) were separated with the Nycodenz density gradient method developed by Apte et al. [38, 119]. In brief, adjacent normal pancreas tissues were achieved from patients with benign pancreatic diseases. After

removing fatty and connective tissue, the tissue was minced to pieces and added with 20mL enzyme solution and 20μL DNase solution (Table 2) for incubation (120 cycles/min, 37°C, 15min). Hereafter, it was filtered by a nylon mesh (100μm), followed by washing twice with GBSS+NaCl solution (Table 2). Cells were resuspended using 9.5mL BSA solution and 8mL Nycodenz solution (Table 2), followed by a 20min centrifugation at 1400g (4°C). Over the above two solutions interface, the fuzzy band was collected in BSA solution and cultured with the complete medium. PSCs were kept in the incubator under standard culture conditions. PSCs were collected for culture or kept in liquid nitrogen after reaching an 80% confluence.

Cell type was verified using immunocytochemical staining for PSCs markers (αSMA, desmin) as described in section 2.2.5. by immunocytochemistry (ICC). PSCs morphology as described by Apte and Bachem[38, 39].

Table 2 Solution formula in PSCs isolation and culture

Solution	Chemicals	Doses
$MgSO_4$ solution	$MgSO_4 \cdot 7H_2O$	0.7g
	DIW	100mL
KH_2PO_4 solution	KH_2PO_4	3g
	DIW	100mL
KCl solution	KCl	3.7g

	DIW	100mL
Na_2HPO_4 solution	$Na_2HPO_4 \cdot 2H_2O$	1.5g
	DIW	100mL
$MgCl_2$ solution	$MgCl_2 \cdot 6H_2O$	2.1g
	DIW	100mL
$CaCl_2$ solution	$CaCl_2 \cdot 2H_2O$	0.0334g
	DIW	100mL
DNase Solution	DNase	10μg
	DIW	1mL
GBSS+NaCl solution	$NaHCO_3$	0.5675g
	D-(+)-Glucose	0.25g
	NaCl	1.75g
	DIW	234.5mL

	$MgSO_4$ solution	2.5mL
	KH_2PO_4 solution	2.5mL
	KCl solution	2.5mL
	Na_2HPO_4 solution	2.5mL
	$MgCl_2$ solution	2.5mL
	$CaCl_2$ solution	2.5mL
GBSS-NaCl solution	$NaHCO_3$	0.1135g
	D-(+)-Glucose	0.05g
	$MgSO_4$ solution	500μL
	KH_2PO_4 solution	500μL
	KCl solution	500μL
	Na_2HPO_4 solution	500μL
	$MgCl_2$ solution	500μL

	$CaCl_2$ solution	500μL
	DIW	47mL
Enzyme solution	Collagenase P	26mg
	Pronase	20mg
	GBSS+NaCl solution	20mL
0.3% BSA solution	BSA	0.15g
	GBSS+NaCl solution	50mL
Nycodenz solution (28.7 %)	Nycodenz	2.87g
	GBSS-NaCl solution	10mL
Complete medium (20%)	DMEM/F12	200mL
	PCN	25000 units
	STR	25mg
	AmB	625μg

	FBS	50mL
Complete medium (10%)	DMEM/F12	180mL
	PCN	20000 units
	STR	20mg
	AmB	500μg
	FBS	20mL

2.2.2. PCCs Culture

Human PCCs (AsPC-1, MIA PaCa-2, PANC-1) were kept by the biobank of our lab and originally from American Type Culture Collection. PCCs were cultivated using RPMI1640 (10% FBS). PCCs were detached employing 0.025% Trypsin/EDTA solution and passaged every two to four days according to cell growth. PCCs were maintained in the incubator under standard culture conditions

2.2.3. Quantitative real-time polymerase chain reaction (qRT-PCR)

2.2.3.1 RNA extraction

After washing cells with PBS three times, RNA extraction was operated following the Qiagen RNeasy Micro Kit protocol. In Brief, cells were resuspended with 350μl RLT

solution. After mixing, the lysate was pipetted to columns arranged within collection tubes, followed by centrifugation (2min, 16000g). 350µl ethanol (70%) was pipetted into lysate and mixed. The mixture was pipetted to new columns in new tubes, followed by centrifugation (15s, 8000g). Flowthrough was abandoned, then 350µl RW1 was pipetted into each column, followed by centrifugation (15s, 8000g). After removal of flowthrough, each membrane of the column was added with 80µl DNase I mix, followed by a 15min incubation at room temperature (RT). Afterward, each column was added of 350µl RW1, followed by centrifugation (15s, 8000g). 500µl RPE was pipetted into columns arranged into clean tubes, followed by centrifugation (15s, 8000g). After removal of flowthrough, the column was added with 500µl 80% ethanol, followed by centrifugation (2min, 8000g). Columns were changed to new tubes, followed by centrifugation (5min, 16000g). Hereafter, columns were placed in tubes, and 14µl RNase-free water was pipetted onto membranes. Finally, after a 1min centrifugation at 16000g, RNA was achieved and kept in a -20°C fridge.

2.2.3.2 Reverse transcription and cDNA pre-amplification

All reagents, like Quantiscript RT and RT Primer Mix, were kept at RT before use, and RNA was thawed on ice. For eliminating genomic DNA, tubes containing the mix (11µL template RNA, 2µL Wipeout buffer, 1µL RNase-free water) were arranged in Thermomixer (42°C, 2min), then immediately placed in the ice box. Hereafter, the mix was pipetted to each tube with another mix (1µl RT Primer Mix, 4µl Quantiscript RT Buffer, 1µl Quantiscript Reverse Transcriptase), followed by incubation (15min, 42°C) for reverse transcription. To inactivate the transcriptase, another 3min incubation (95°C) of tubes was applied. Finally, cDNA was then prepared directly for experiments or kept in a fridge (-80°C).

2.2.3.3 qRT-PCR array using the SYBR green method

qRT-PCR allows the PCR progress to be examined during its execution. The fluorescence detection includes an intercalating reagent (SYBR Green I) which fluoresces as it bounds to double-stranded DNA. The DNA-SYBR Green complex is stimulated at 494nm, then releases green light at 520nm. The quantitative determination of target DNA is realized by examining the fluorescence. A total of 42 PCR cycles consisting of an initial denaturation cycle (95°C, 5min), 40 cycles for primer hybridization (95°C, 10min) and elongation (60°C, 30min), and a melting cycle (heated from 60 to 95°C within 6min). The fluorescence is detected at the end of the elongation phase in each of the 40 primary cycles. The fluorescence increases in proportion to the PCR reaction and can thus be used to evaluate the amount of the corresponding nucleic acids. A threshold for the level of fluorescence is set, and a threshold cycle (Ct) means the number of cycles at which fluorescence reaches a threshold. Besides, the GAPDH gene is determined as the reference gene to make relative quantification possible. ΔCt is the difference of Ct_{GAPDH} to Ct value of the target gene. Relative values of target genes are calculated using $2^{-\Delta Ct}$, since the DNA doubles for each cycle at 100% amplification efficiency, which is an exponential multiplication.

2.2.4. Proliferation Assay

Proliferation detection was conducted applying a commercially available EZ4U kit, a modified MTT assay. To be short, PSCs or PCCs ($1x10^4$ cells/well) were cultured using a complete medium (200μL/well). One day after seeding, new medium with different treatments was applied to replace the old one. For the PSCs proliferation testing, PSCs were pretreated with 100nM Cal or DMSO for 48h. For PCCs proliferation testing, PCCs were cultured with the conditioned medium of cancer-associated PSCs (pretreated with or without 100nM Cal) for 48h. Each well was added with a 20μL dye

substrate, followed by a three h incubation. A microplate reader, setting at 450nm, was applied to determine the absorbance.

2.2.5. Immunocytochemistry (ICC)

Standard ICC protocol was followed to stain the cells using the mouse mAb against desmin or αSMA. Briefly, 4% paraformaldehyde-fixed PSCs (treated with or without 100nM calcipotriol) slides were rinsed twice using PBS and soaked within 1.5% H_2O_2/PBS solution for 15min in the dark. Following two 5min PBS washes on a shaker, slides were incubated with 5% BSA into each well to block at 4°C for 12h in a humid atmosphere. Slides were incubated using mouse primary mAb against desmin and αSMA (1h, RT). Following another three washes, slides got incubated using HRP-linked secondary Ab (1h, RT). After washing, they were incubated applying 3,3'-diaminobenzidine (DAB) and immediately washed with PBS twice after color development. Counterstaining was conducted using hematoxylin for 30s, followed by two PBS washes. Cover slips with a Dako pen and observe slides under a light microscope.

2.2.6. Wound Healing (WH) Test

For investigation of PSCs migration ability, a standard WH test protocol was applied. Briefly, PSCs ($5x10^5$ cells/well) were grown in plates until 100% confluence under standard culture conditions. Utilizing a 200μL tip, cell monolayers were scratched manually through the center of each well, eliminating cells from an area with about 0.5mm width. After two washes, PSCs were removed of cellular debris and cultured within fresh medium with or without 100nM calcipotriol. Photos were taken every 12h within 60h under a light microscope (magnification: 100x). The wound area was calculated by Image J and utilized for statistical analysis.

2.2.7. Migration and Invasion Assessment

Migration and invasion were tested by conducting experiments applying transwell chambers in the absence or presence of Matrigel. For PSCs migration investigation, PSCs were firstly cultured in the medium with 1% FBS for 24h. $5x10^4$ PSCs were then suspended in 200μL medium (with or without 100nM calcipotriol) and pipetted into each upper chamber. For each lower chamber, 600μL DMEM/F12 with 5% FBS was arranged as a chemoattractant. As to PSCs-PCCs coculture, PSCs ($1x10^5$ cells) treated with or without 100nM Cal were grown in each lower chamber. 24h after seeding, fresh medium was applied to replace the old. PCCs ($5x10^4$ cells) with 200μL medium were pipetted into each upper chamber. The incubation time of migration or invasion experiments is 24h and 48h, respectively. Hereafter, cells staying on the upper side of the membrane were eliminated manually. Besides, crystal violet was utilized to stain the cells which invaded or migrated to the lower side. Quantitative determination was done by calculating cells within ten random fields using a light microscope (magnification 200x).

2.2.8. Western Blot (WB)

2.2.8.1 Extraction of proteins from adherent cells

After three PBS washes, cells were added with RIPA lysis solution. Using cold plastic scrapers, cells were scraped and further collected into microfuge tubes. After 30min agitation, microfuge tubes were centrifuged (16000g, 20min, 4°C). Finally, new tubes were applied to collect supernatant and placed in an ice box.

2.2.8.2 Quantitation of protein

BCA Protein Assay Kit was applied in protein quantitation. Following the

manufacturer´s protocol, standard or target proteins (25µl) were arranged into every well. Afterward, a 200µl reagent mixture (reagent A: reagent B=50:1) was pipetted into each well. Hereafter, the plate was agitated carefully on a shaker for 30s. Following incubation (37°C, 30min), absorbance (562nm) was detected by applying a plate reader. The standard curve based on standard proteins was available by plotting average blank-adjusted readout versus concentration (µg/mL).

2.2.8.3 Immunoblotting

2.2.8.3.1 Polyacrylamide gel preparation

Glass, as well as spacers, were cleaned using ethanol and deionized water. Clean glass sheets were assembled with spacers on a flat desktop. 10mL resolving gel solution (Table 3) was poured into the glass sheets with spacers. The resolving gel was overlaid with isopropanol and left for 20-30min at RT to keep a flat and horizontal surface. Overlaid isopropanol on resolving gel was then discarded, and stacking gel solution (Table 3) was added until it spilled over. A comb was instantly inserted without air bubbles between the gel and comb. It will take around 30min at RT to set gel.

2.2.8.3.2 Polyacrylamide gel electrophoresis

Samples including equivalent volumes of proteins (20µg/lane), including a weighted marker in one of the lanes, were carefully pipetted to SDS-PAGE wells. Electrophoresis equipment was added with running buffer (1x, see Table 3) according to the manufacturer. Hereafter, the gel was run as instructed by the manufacturer at 100V for 1h.

2.2.8.3.3 Membrane transfer

Methanol was applied to stimulate PVDF membranes for 25s to get stimulated. Membranes were soaked in transfer buffer for use (1x, see Table 3). The membranes were dealt with carefully using a rounded tweezer to avoid scratching or puncturing the surface. Filter papers and sponges were put into transfer buffer 5min before “sandwich” creation. Following electrophoresis, the gel was separated from the machine for the transfer sandwich preparation. The sandwich layers were sequentially assembled, carefully getting rid of any air bubbles with a pipette since they will interrupt the procedure of protein transfer. Finally, the sandwich was put in the transfer container, and a wet transfer was conducted as instructed by the manufacturer’s protocol.

2.2.8.3.4 Immunoblotting

Following the transfer, TBST (1x) was applied to wash membranes three times. Blocking solution (Table 3) was utilized to incubate membranes overnight with continuous shaking (4˚C). Primary mAb solution was made by diluting to working concentration as recommended by the manufacturer’s protocol in TBST (1x) with 1% milk. The membranes were put into primary mAb solution with gently shaking (2h, RT). The membranes were placed in a secondary antibody solution (mild rocking, 1h, RT). Lastly, membranes were ready for detection following three washes.

2.2.8.3.5 Detection

According to the manufacturer's guidelines, the membrane was incubated for 3min in the ECL substrate, made before use. Hereafter, it was exposed to autoradiography film in a dark room. The grey values of bands were calculated by image J and used for further statistical analysis.

Table 3 Solution formula in WB

Solution	Chemicals	Doses
Resolving gel solution	deionized water (DIW)	3.8mL
	1.5M Tris-HCl (pH 8.8)	2.6mL
	30% Arc	3.4mL
	10% SDS	0.1mL
	TEMED	0.01mL
	10% APS	0.1mL
Stacking gel solution	DIW	5.86mL
	1.5M Tris-HCl (pH 6.8)	2.6mL
	30% Arc	1.34mL
	10% SDS	0.1mL

	TEMED	0.01mL
	10% APS	0.1mL
Running Buffer (10x)	Tris Base	30g
	Gly	144g
	SDS	10g
	DIW	1L
Running Buffer (1x)	Running Buffer (10x)	0.1mL
	DIW	0.9mL
Transfer Buffer (10x)	Tris Base	30g
	Gly	144g
	DIW	1L
Transfer Buffer (1x)	Transfer Buffer (10x)	0.1L
	Methanol	0.1L

	DIW	0.8L
TBS (10x)	Tris Base	24g
	NaCl	80g
	DIW	1L
	PH	7.6
TBST (1x)	TBS (10x)	0.1L
	DIW	0.9L
	Tween 20	1mL
Protein lysis Buffer	RIPA buffer	0.1L
	Protease inhibitor	One tablet
Tris-HCl (1M) solution	Tris-base	12.12g
	DIW	0.2L
	PH	6.8

Tris-HCl (1.5M) solution	Tris-base	36.34g
	DIW	0.2L
	PH	8.8
Loading buffer	loading buffer (4x)	0.9mL
	β-Mercaptoethanol	0.1mL
SDS solution (10%)	SDS	10g
	DIW	0.1L
APS solution (10%)	APS	10g
	DIW	0.1mL
Blocking solution	Milk powder	1g
	TBST (1x)	20mL

2.2.9. Statistical Analysis

SPSS 21.0 package was applied in all statistical analyses. The standard deviation of the mean (SD) represented the variance of mean values. Student t-test was used in the determination of differences between groups. Data in figures were exhibited as mean±SD of minimum triplicate or independent experiments. Chi-Squared tests were utilized to evaluate the correlation between VDR and αSMA expression. P-value (<0.05) was of statistical significance.

3. Results

3.1. Establishment, verification of isolation of both activated and quiescent PSCs

3.1.1 Establishment of PSCs isolation

Using the outgrowth method, the cancer-associated PSCs (caPSCs) and chronic pancreatitis-associated PSCs (cpPSCs) were isolated from fibrotic parts of the pancreas, which were resected from PDAC or CP patients. The activated PSCs (caPSCs and cpPSCs) emerged from tissue blocks 3-5 days after seeding in the uncoated plastic cell culture plates (Figure 3A, Table 3). Morphologically, the activated PSCs showed a myofibroblast-like phenotype with a star-like shape and no lipid droplets inside (Figure 3A).

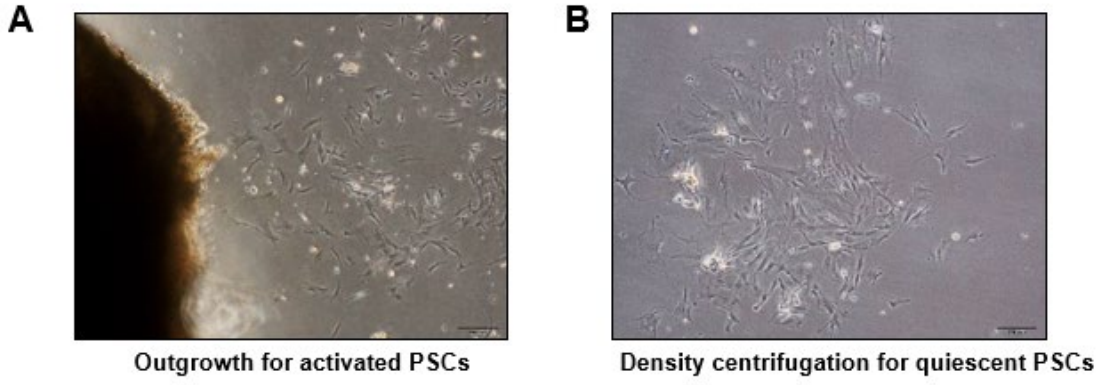

Figure 3: Activated or quiescent PSCs were isolated using different methods. Representative photos: (A) with the outgrowth method, typical activated PSCs emerged from tissue block 3-5 days after seeding. Magnifications (x100). (B) nPSCs were isolated from normal pancreas utilizing the density centrifugation method. Magnifications (x100).

However, no normal PSCs (nPSCs) grew out from normal pancreas tissue block using the outgrowth method, and this was similar to the result of Bachem's[39]. The nycodenz density centrifugation method, described by Apte[38], was then utilized in histologically confirmed normal pancreatic tissues, and the yield of nPSCs was regularly 0.3-1.6x10^6/g (Figure 3B, Table 3). The viability of all three kinds of PSCs was over 90% as evaluated with trypan blue staining (Table 3).

Table 3 Details of isolated PSCs from different tissue types

	Normal pancreas	**Pancreatic cancer**	**Chronic pancreatitis**
Isolation method	Density centrifugation	Outgrowth	Outgrowth
Tissue weight (g)	0.14-3.52	0.2-1.22	0.36-1
Isolation times	35	8	6
Yield (x 10^6/g)	0.3-1.6	/	/
Emerging Timepoint	/	3-5 days	3-5 days
Viability	>90%	>90%	>90%
Doubling time	29.9±4.1h	27.7±3.7h	28.6±3.7h

"/": For PSCs isolated from pancreatic cancer and chronic pancreatitis, it's unable to measure the yield directly because activated PSCs slowly emerge from tissue block and proliferate over time. For PSCs isolated from the normal pancreas, emerging timepoint is not applicable as PSCs are isolated directly from tissue block, and the yield can be measured immediately.

Morphologically, freshly separated nPSCs indicated an irregular shape with abundant perinuclear lipid droplets (Figure 4A), similar to the previous report by Apte in 1998[38]. After treated with trypsin for the 1st passage, all nPSCs transformed into the activated myofibroblast phenotype, which lost typical lipid droplets and showed a stellate-like shape (Figure 4B). nPSCs that subsequently passed during culture appeared not apparent morphological difference compared with the activated PSCs obtained by outgrowth.

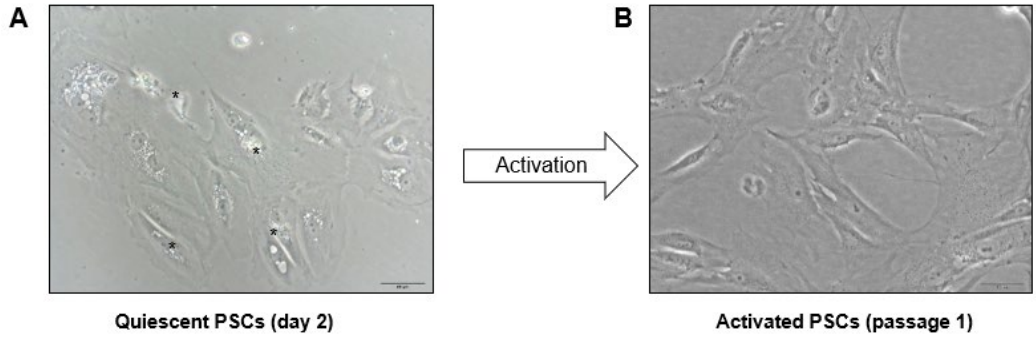

Figure 4: Morphology change in PSCs activation. Representative photos: (A) Newly isolated PSCs showed a quiescent phenotype that exhibited an irregular polygonal appearance with perinuclear lipid droplets (asterisks). (B) After the first passage, nPSCs turned into an activated phenotype that lost lipid droplets and changed into star-shaped cells.

It was observed that most nPSCs attached to the flasks between 20h and 36h following seeding. The doubling time of the different kinds of PSCs (established from 5 separate nPSCs, caPSCs, and cpPSCs, between 3rd and 5th passage) was 29.9±4.1h, 27.7±3.7h, and 28.6±3.7h, respectively (Table 3, Figure 5). Therefore, no difference in the cell growth velocity between PSCs from different origins has been detected.

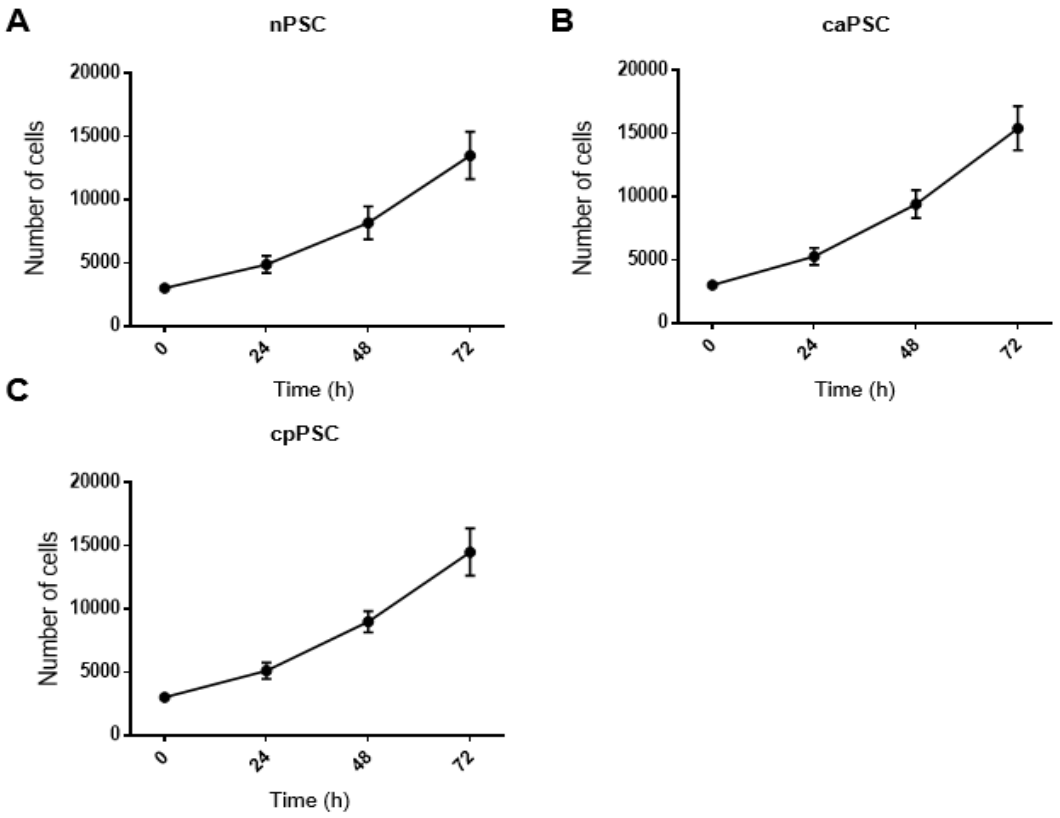

Figure 5: Growth curve of three different kinds of PSCs. The doubling time of nPSCs (A), caPSCs (B), cpPSCs (C) was 29.9±4.1h, 27.7±3.7h, and 28.6±3.7h, respectively.

Compare to the data reported by other papers[8, 38, 39, 119], the results presented in our study are similar in terms of cell morphology, yield, viability, and growth curve. Overall, both the density centrifugation method for quiescent PSCs and the outgrowth method for activated PSCs isolation is well established in this project.

3.1.2 PSCs verification

αSMA has already been widely recognized as an excellent marker of activated PSCs both in-vitro and in-vivo[6, 38, 39, 42, 119]. In this part, cells were further verified as PSCs using immunocytochemistry staining for the PSCs activation marker αSMA and selective marker desmin between passages 1 and 3.

It was noticed that αSMA with immunocytochemistry staining showed the strongest immunoreactivity as 100% of cells indicated strong cytoplasmic positivity (Figure 6B), which further supported the opinion that αSMA was a perfect marker of activated PSCs[6, 43]. In comparison, 40-55% of cells showed a cytoplasmic positivity for desmin (Figure 6C), consistent with previous research that desmin was not expressed in all activated PSCs[38, 39].

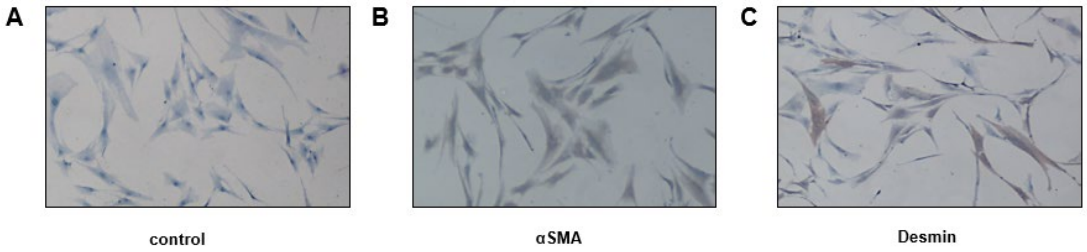

Figure 6: Isolated cells were confirmed as PSCs by ICC staining of PSCs activation marker αSMA and selective marker desmin. Representative photos: (A) negative control. Magnifications (x100). (B) ICC observed positive staining of αSMA in PSCs (passage 1). Magnification (x100). (C) Positive staining for desmin by ICC in PSCs (passage 1). Magnification (x100).

In conclusion, with the ICC staining of the widely accepted PSCs activation marker αSMA, the isolated cells are confirmed as PSCs with high purity in this project. The isolation technologies are reliable for further experiments.

3.2. Expression of VDR is higher in caPSCs than PCCs

There were already several pieces of research showing that mouse cpPSCs highly expressed VDR in the mouse chronic pancreatitis model[79, 120, 121]. However, little evidence about VDR expression of caPSCs and PCCs was found in human pancreatic cancer. This project assessed the VDR mRNA level and activity of this receptor in human caPSCs and PCCs.

VDR expression was evaluated by qRT-PCR in 3 caPSCs samples and 3 PCCs (AsPC-1, MIA PaCa-2, PANC-1). In Figure 7A-B, caPSCs showed a relatively higher VDR expression than PCCs (p=0.014). For the VDR activity evaluation, 100nM calcipotriol (cal), a potent vitamin D analog [79], was applied to stimulate VDR for 48h. CYP24A1, markedly inducible when the VDR ligand binds to VDR[122], was assessed by qRT-PCR as a readout for activation of VDR. After the treatment of the VDR ligand, caPSCs consistently responded to the VDR ligand and expressed higher CYP24A1 than the control group (p=0.001). However, PDAC lines showed a typically low VDR activity and low CYP24A1 expression after VDR ligand treatment (p=0.145) (Figures 7C-D).

These findings demonstrated that caPSCs showed a relatively high expression of VDR and reacted to VDR ligand, while PCCs exhibited differing low VDR expression and activity.

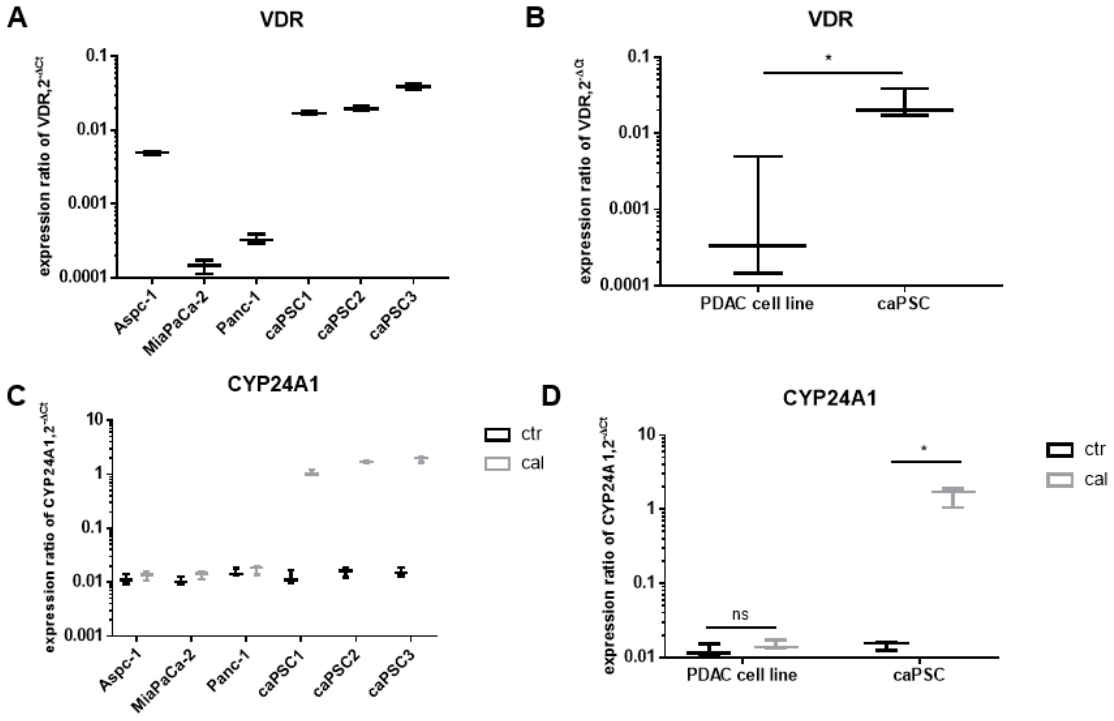

Figure 7: CaPSCs expressed higher VDR and reacted to Cal, while PCCs exhibited lower VDR and activity.

(A)(B) qRT-PCR was utilized to evaluate VDR expression in three PCCs and three caPSCs. (unpaired t-test, * $p<0.05$). (C)(D) Indicated PCCs or PSCs with DMSO or Cal (100nM, 48h). qRT-PCR was applied to assess CYP24A1 expression, and values were normalized to GAPDH. (paired t-test, * $p<0.05$).

3.3. VDR induction by its ligand decreases the PSCs activation

Several pieces of research on hepatic fibrosis have verified that VDR induction decreased fibrosis, which was mainly caused by activated HSCs[11, 12, 14]. In addition, VDR ligand induction in fibroblast was reported to reduce lung fibrosis[10, 123] and renal fibrosis[13, 124, 125]. These researches inspired us to hypothesize that VDR might have the potential of deactivating PSCs and reducing fibrosis. This part will mainly explore the functions of this druggable receptor in PSCs activation.

3.3.1. Vitamin D analog reduces αSMA expression in PSCs

We respectively conducted ICC, WB, and qRT-PCR to investigate VDR's role in PSCs activation.

For the immunocytochemistry evaluation, caPSCs were incubated with 100nM Cal or vehicle (DMSO) for 48h, and αSMA staining was employed. The proportion of αSMA-positive caPSCs was nearly 100% in the vehicle-treated group, while this proportion significantly decreased to 27% in the 100nM Cal-treated caPSCs group by ICC staining (p=0.000) (Figure 8). This result indicated that VDR induction by its ligand opposed caPSCs activation.

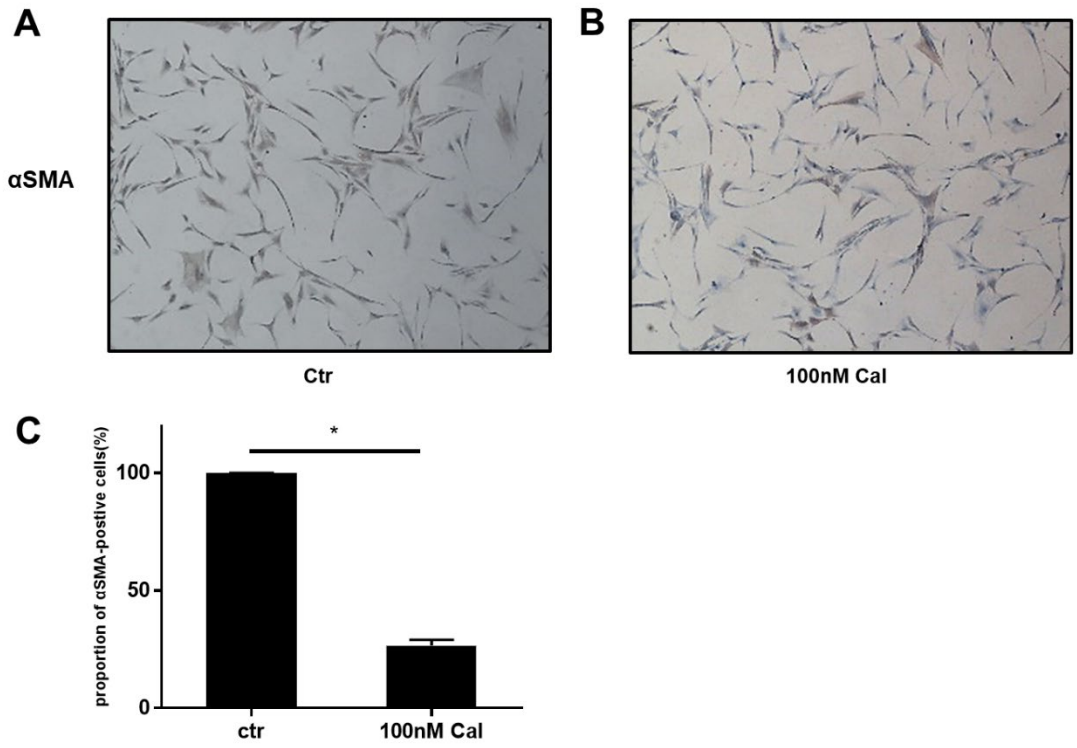

Figure 8: VDR induction by its ligand reversed caPSCs activation evaluated by ICC. (A)(B) Representative photos: αSMA expression was measured by ICC in the three caPSC samples incubated with vehicle (A) or Cal (B) for 48h. (C) Quantification analysis of the proportion of αSMA-positive cells in caPSCs treated with or without 100nM Cal. (paired t-test, * $p<0.05$).

WB was then performed to further confirmed the above result at the protein level. Compared to the control group, 100nM Cal-treated caPSCs showed a higher expression of VDR (p=0.003) and lower αSMA expression (p=0.004) in four caPSCs samples (Figure 9). This strongly supported our hypothesis that the activation procedure of caPSCs was reversible by VDR induction of ligand.

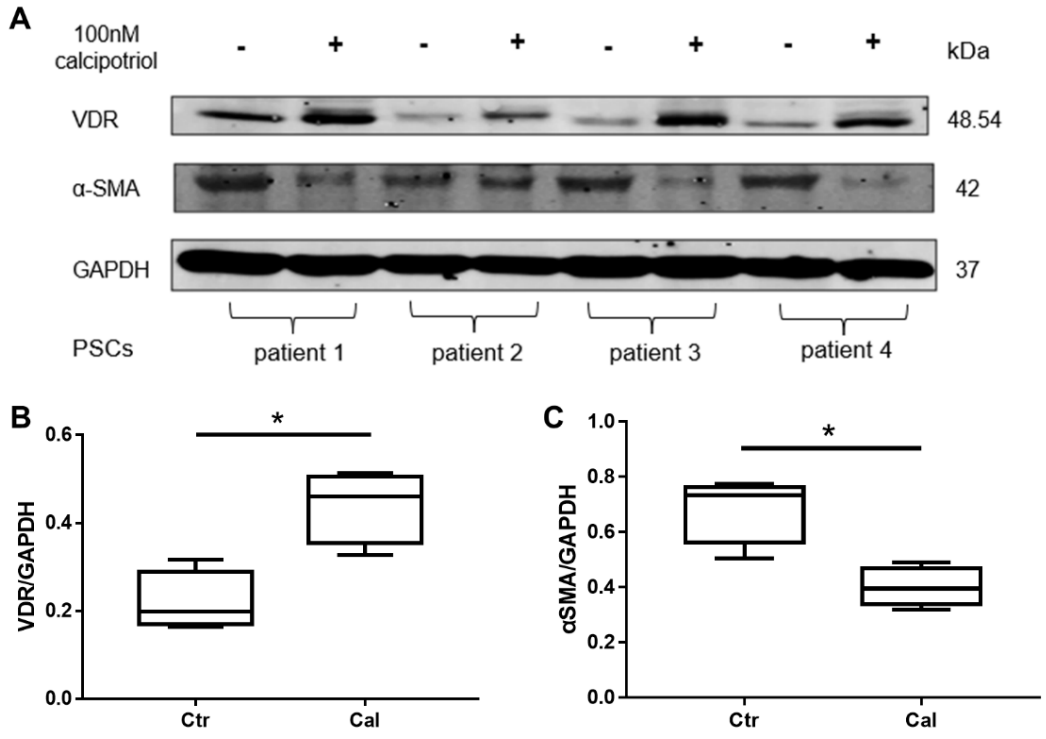

Figure 9: VDR induction by 100nM Cal promoted caPSCs deactivation. (A) WB showed protein expression of VDR and αSMA in four caPSCs samples in the absence or presence of 100nM Cal. (B)(C) Compared to the control group, 100nM Cal-treated caPSCs showed a higher expression of VDR and lower αSMA expression in caPSCs. (paired t-test, * $p<0.05$, ** $p<0.01$).

Furthermore, this effect was evaluated in three different kinds of PSCs, and the correlation between VDR and αSMA was investigated at the mRNA level.

qRT-PCR was conducted in three different kinds of PSCs (caPSCs, cpPSCs, nPSCs), treated with or without 100nM Cal. Similar to the results shown in ICC and WB, VDR mRNA expression significantly increased (p=0.002, 0.022, 0.024, respectively), while αSMA decreased in all three kinds of PSCs (caPSCs, cpPSCs, nPSCs) after 100nM Cal treatment (p=0.012, 0.001, 0.005, respectively)(Figure 10A-B). Correlation analysis indicated that VDR was in a moderate negative correlation with αSMA expression (p=0.031, Pearson's r=0.641)(Figure 10C).

Overall, VDR plays a significant role in the PSCs activation procedure. In addition, with the capability to decrease the activation of PSCs, VDR induction by its ligand is expected to become a promising anti-stroma strategy of PDAC therapy.

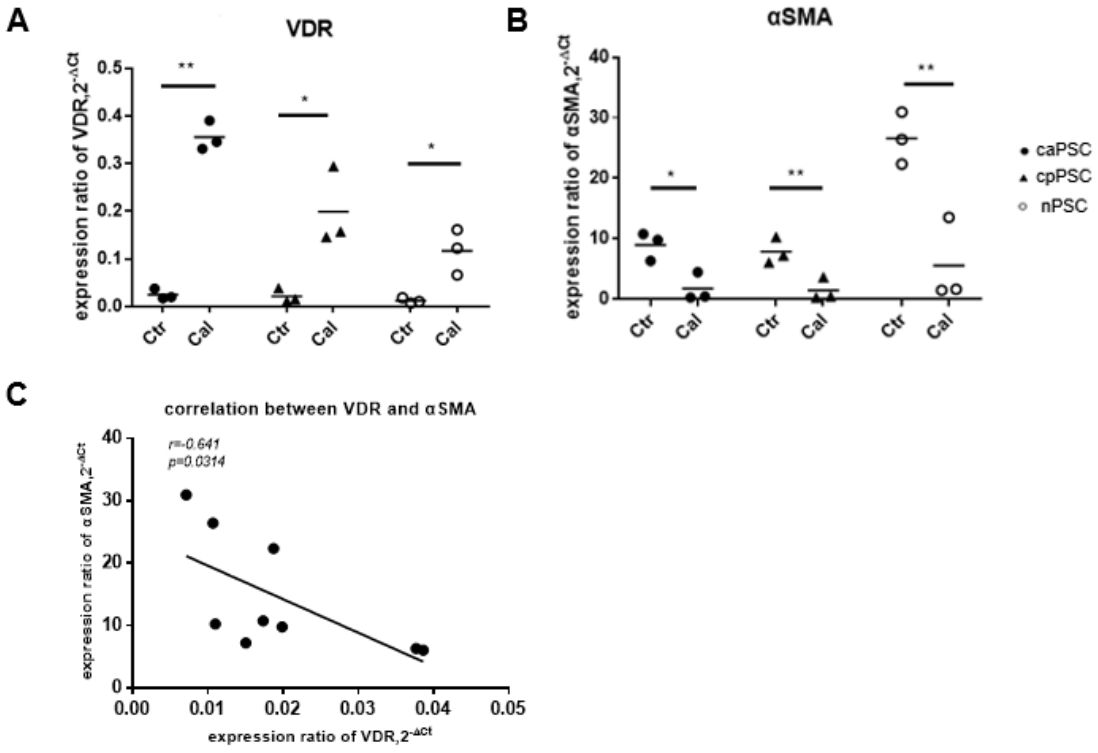

Figure 10: VDR and αSMA mRNA expression in 3 different kinds of PSCs treated with vehicle or 100nM Cal. (A)(B) qRT-PCR was applied to measure VDR and αSMA expression in caPSCs, cpPSCs, and nPSCs samples. (paired t-test, * $p<0.05$). (C) VDR was indicated to be in a moderate negative correlation with αSMA expression in correlation analysis,.

3.3.2. Vitamin D analog decreases migration ability of activated PSCs

Migration ability was firstly reported as another feature of activated PSCs by Phillips in 2003[126] and verified by several other researchers [127-130]. PSCs have been reported to have the ability to migrate in reaction to chemokines like PDGF[126]. In addition, PSCs showed the ability to migrate when exposed to cancer cell secretions[6]. We supposed that the VDR ligand decreases the migration ability of activated PSCs. Therefore, in this part, the WH test and transwell experiments were conducted to explore whether VDR induction by its ligand could influence the migration ability of caPSCs or not.

In the wound healing assay, scratched caPSCs ($5x10^5$ cells/well) monolayers were cultured with 100nM Cal or vehicle, and photos were taken at different timepoints as described in 2.2.6. Figure 11 showed that, wound area of caPSCs treated with 100nM Cal healed slower than the untreated control group from 24h (p values for 12h, 24h, 36h, 48h, 60h were 0.499, 0.010, 0.001, 0.000, 0.000, respectively). This result suggested that VDR activation decreased the migration ability of caPSCs.

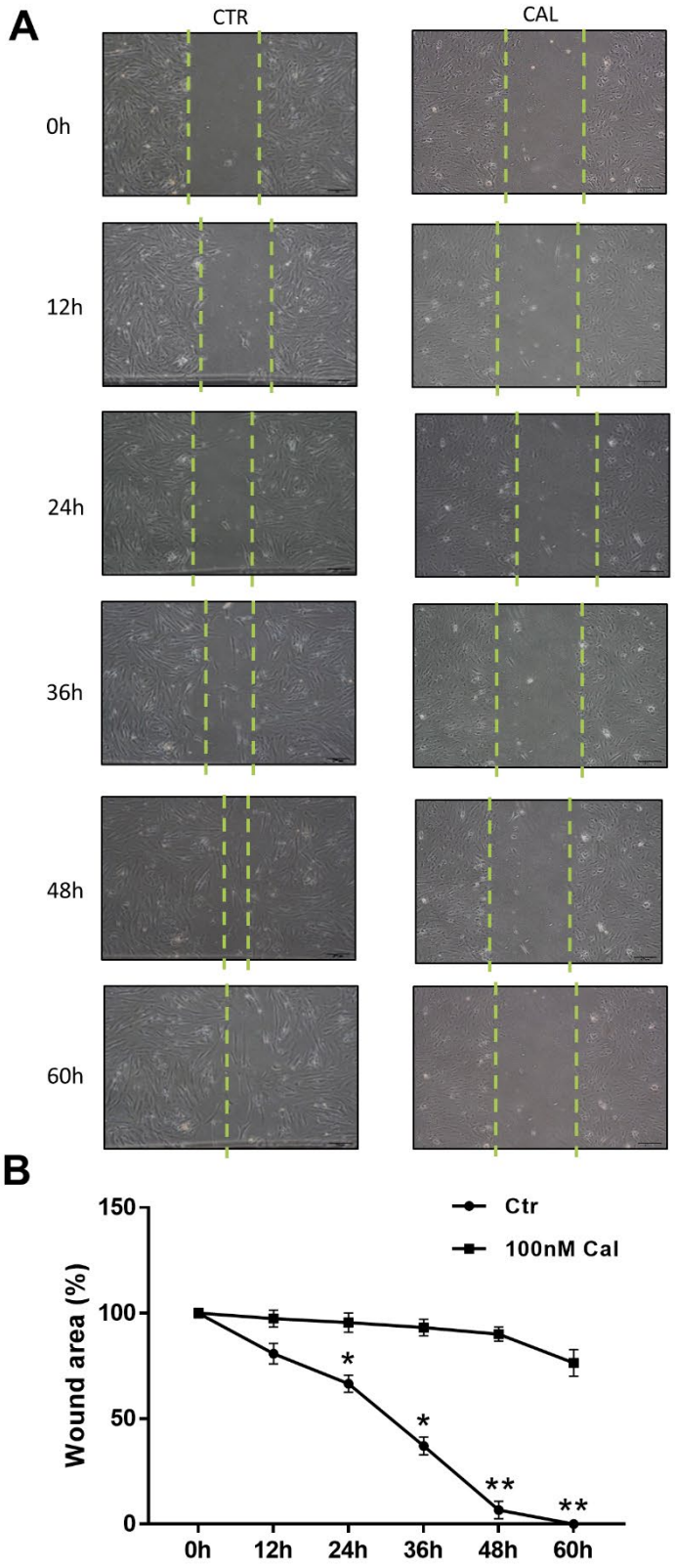

Figure 11: VDR ligand decelerated migration ability of caPSCs in WH assay. The migration ability was evaluated by the WH test in caPSCs. caPSCs were treated with or without 100nM Cal as described in 2.2.6. Results were obtained by conducting independent experiments three times, and pictures were obtained under a light microscope at different time points (magnification: x200). ** p<0.01, * p<0.05.

A Transwell migration assay was also conducted to confirm the result further. CaPSCs were firstly cultured in medium (1% FBS) for 24h, and $5x10^4$ caPSCs were suspended in 200μL medium with 100nM Cal or vehicle and grown in upper chambers. 600μL DMEM/F12 (5% FBS), as a chemoattractant, was pipetted into lower chambers.

As shown in Figure 12, 100nM Cal treated group showed a statistically significantly smaller number of cells that passed through the membrane than the control group after 24h (p=0.000).

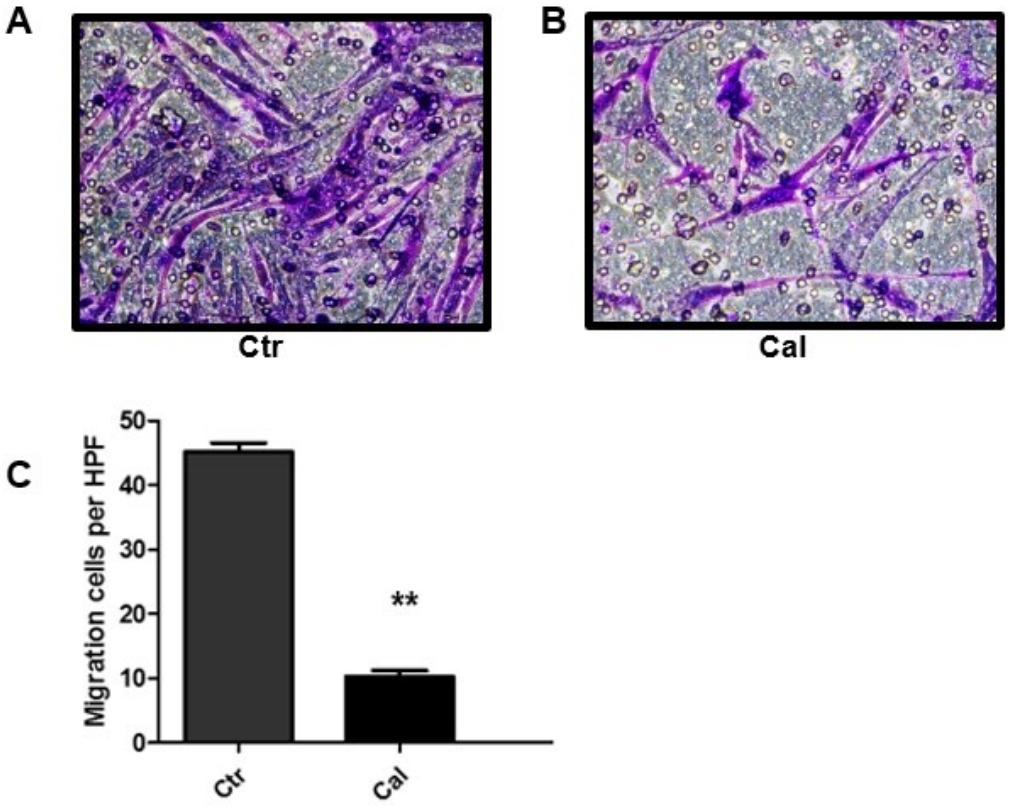

Figure 12: VDR ligand reduced the migration ability of caPSCs in the transwell migration assay. (A) (B) Representative photos of transwell migration assay for caPSCs in the absence (left) or presence (right) of 100nM Cal. (C) Quantification of transwell migration experiment showed the effect of 100nM Cal on the migration capability of caPSCs. Photos were taken by light microscopy (x 200 magnification) after 24h. Quantification was conducted by calculating cells in ten random fields. HPF: high-powered fields. ** $p<0.01$, * $p<0.05$.

3.3.3. Vitamin D analog decreases proliferation ability of activated PSCs

Proliferation ability is widely accepted as the feature of activated PSCs[8, 9, 131, 132]. Freshly isolated nPSCs from histologically normal pancreas and caPSCs from tumor tissue were cultured with 100nM Cal or DMSO in 96-well plates for 48h. EZ4U was applied to evaluate the proliferation ability of PSCs following the manufacturer´s protocol. As indicated in Figure 13, the VDR ligand reduced the proliferation ability of caPSCs (p=0.000), while this effect was not found in the nPSCs group (p=0.829).

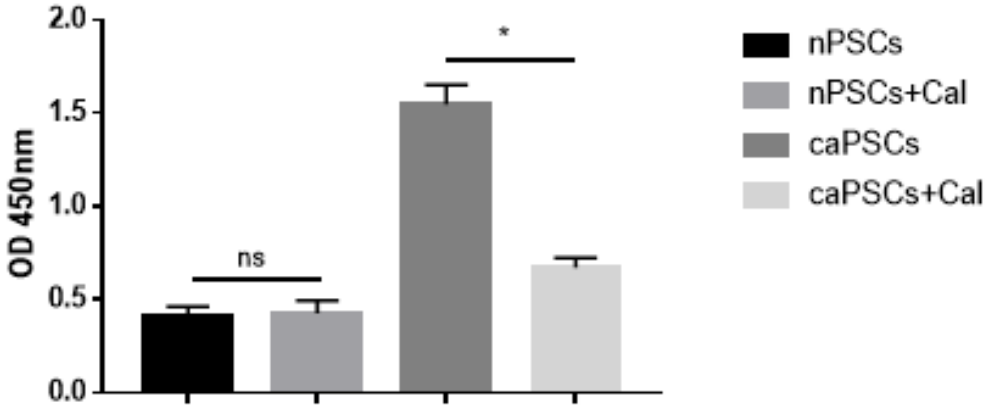

Figure 13: VDR induction decreased the proliferation of caPSCs but not that of nPSCs. nPSCs and caPSCs were incubated with or without 100nM Cal, and proliferation ability was assessed by EZ4U assay (paired t-test, * p<0.05, ns=not significant).

3.4. VDR activation in caPSCs attenuates caPSCs-augmented progression of PCCs

Several studies indicated that caPSCs enhanced the proliferation, migration, and invasion ability of PCCs[59, 133-135]. Therefore, we put forward the hypothesis that VDR activation in caPSCs might attenuate caPSCs-augmented proliferation, migration, and invasion ability of PCCs. Thus, in this part, we assessed the influence of VDR ligand-stimulated caPSCs on the interplay between caPSCs and PCCs.

3.4.1. VDR activation in caPSCs decreases caPSCs-augmented migration ability of PCCs

To evaluate the impact of VDR activation in caPSCs on migration ability of PCCs, transwell migration experiments were carried out utilizing chambers without coated Matrigel. Three caPSCs were grown to confluency, followed by a 100nM Cal or DMSO treatment for 48h. The caPSCs above were co-cultured with the PCCs (AsPC-1, PANC-1, MIA PaCa-2) in a transwell co-culture system for 24h. As shown in Figure 14, PCCs co-cultured with deactivated caPSCs (pretreated with 100nM Cal) showed a weaker migration ability than the control ($p=0.001$, 0.000, 0.004). Results demonstrated that VDR-stimulated caPSCs decreased the caPSCs-augmented migration ability of PCCs.

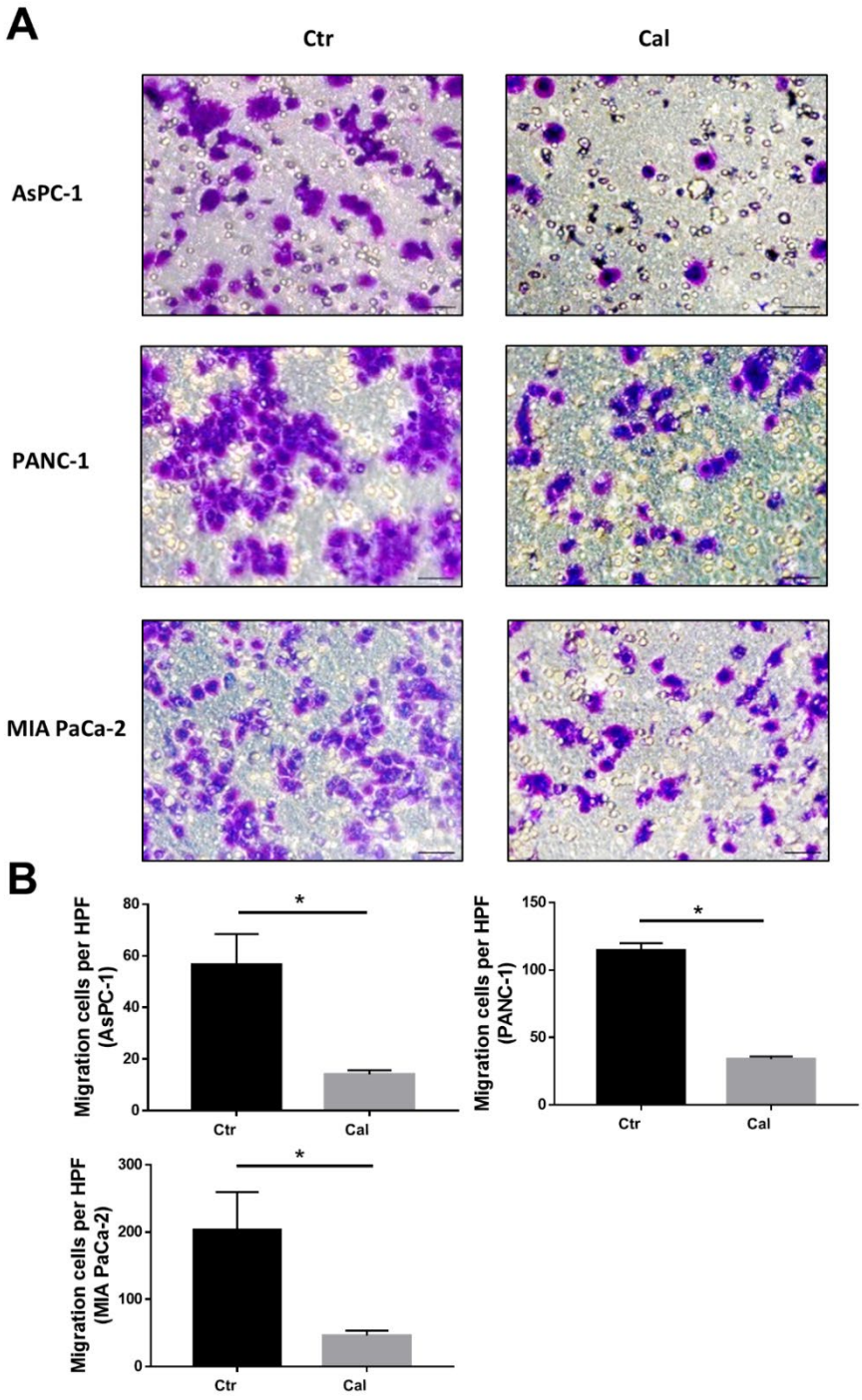

Figure 14: VDR activation in caPSCs decreased caPSCs-augmented PCCs migration. (A) Representative photos: three PDAC cell lines were co-cultured with three caPSCs samples (pretreated with or without 100nM Cal for 48h) in a transwell co-culture system for 24h. Cells migrating onto the lower side were stained using crystal violet. (B) PCCs co-cultured with deactivated caPSCs (pretreated with 100nM Cal) showed a weaker migration ability than the control. HPF: high-powered fields. (paired t-test, * $p<0.05$).

3.4.2. VDR activation in caPSCs decreases caPSCs-augmented invasion ability of PCCs

To assess the effects of VDR activation in caPSCs on the invasion ability of PCCs, transwell invasion experiments were performed utilizing chambers coated with Matrigel. Three caPSCs were grown to confluency, followed by a 100nM Cal or DMSO treatment for 48h. The caPSCs above were co-cultured with the PCCs (mentioned in 3.4.1) were then co-cultured in a transwell co-culture system for 48h. As presented in Figure 15, PCCs cultured with deactivated caPSCs (pretreated with 100nM Cal) indicated a weaker invasion ability than that of control (p=0.000, 0.000, 0.000). The results proved that VDR-stimulated caPSCs diminished the caPSCs-augmented invasion ability of PCCs.

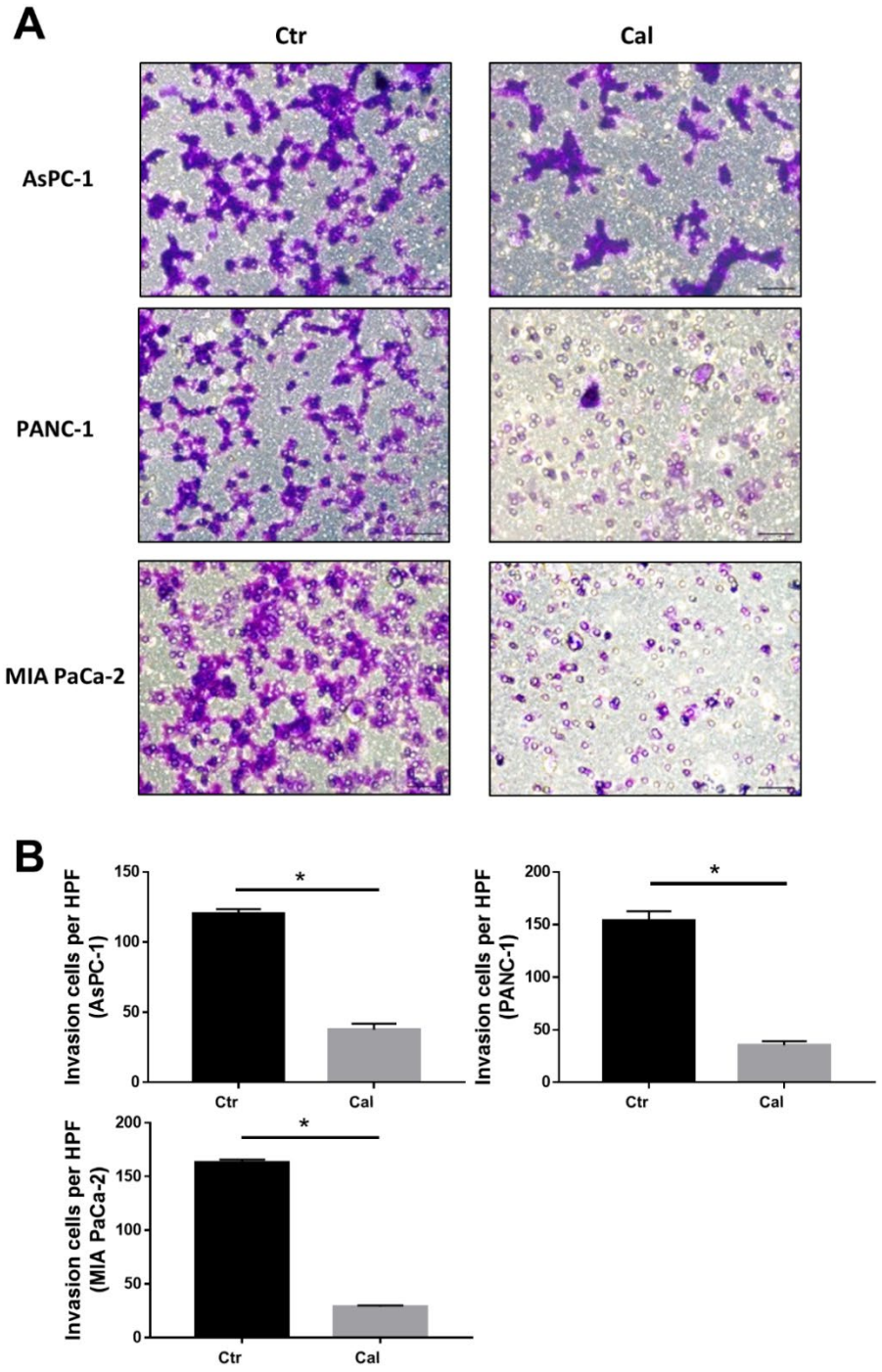

Figure 15: VDR activation in caPSCs decreased caPSCs-augmented PCCs invasion. (A) Representative photos: three PDAC cell lines were co-cultured with three caPSCs samples (pretreated with or without 100nM Cal for 48h) in a transwell co-culture system for 48h. PCCs invading onto the lower side were stained using crystal violet. (B) PCCs cultured with deactivated caPSCs (pretreated with 100nM Cal) indicated a weaker invasion ability than control. HPF: high-powered fields. (paired t-test, * $p<0.05$).

3.4.3. VDR activation in caPSCs diminishes caPSCs-augmented proliferation ability of PCCs

Finally, the effect of calcipotriol-treated caPSCs on the proliferation of PCCs was determined in accordance with the manufacturer´s protocol of the EZ4U assay.

Three primary caPSCs were grown to confluency and incubated with 100nM Cal or vehicle for 48h. Conditioned medium (CM) from them was gathered and transferred to culture different PCCs grown in 96-well plates for 48h. Figure 16 showed that, CM from deactivated caPSCs (pretreated with 100nM Cal) significantly decreased proliferation ability of all three PCCs ($p=0.007$, 0.008, 0.002 for AsPC-1, PANC-1, MIA PaCa-2 respectively). However, this effect was not observed in all three PCCs incubated with CM from the activated caPSCs, pretreated with vehicle ($p=0.714$, 0.304, 0.098 for PCCs mentioned above). Results showed that VDR activation in caPSCs negatively regulated the caPSCs-augmented proliferation of PCCs.

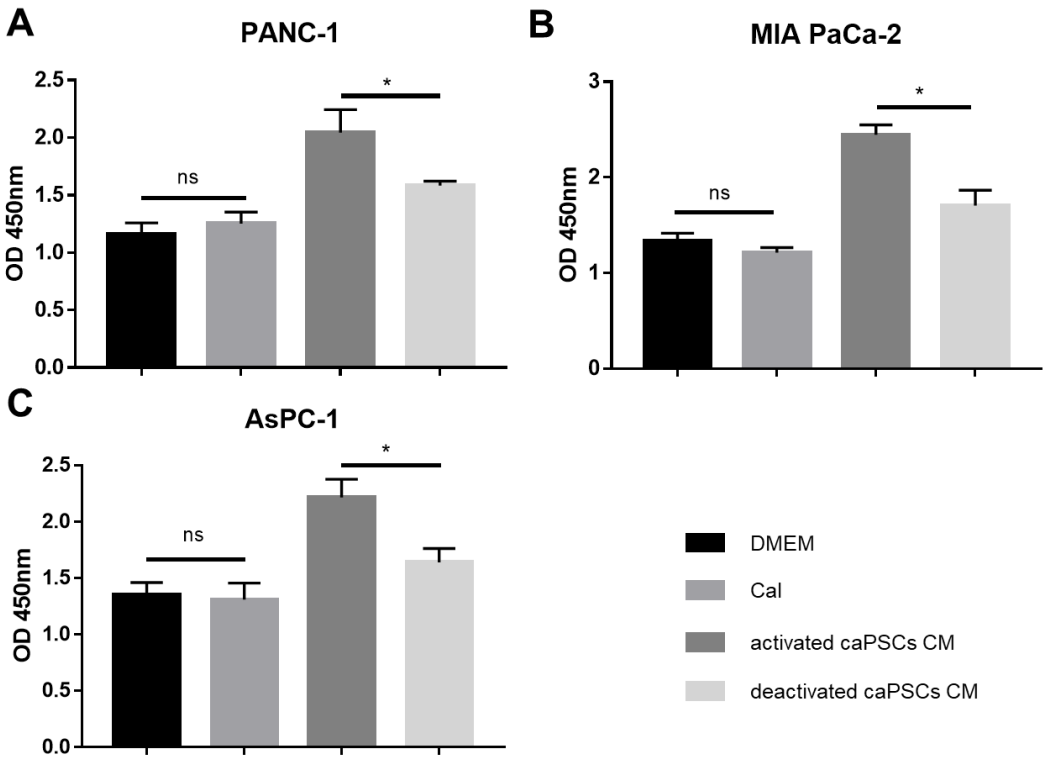

Figure 16: VDR activation in caPSCs decreased caPSCs-augmented PCCs proliferation. The PDAC cell lines were cultured in CM from three caPSCs samples (pretreated with or without 100nM Cal for 48h) in a 96-well plate for 48h. 20µL dye substrate was then pipetted into each well, followed by a 3h incubation. Absorbance as described in 2.2.4. (paired t-test, ns=of no significance, * $p<0.05$).

4. Discussion

With well-established isolation technologies, VDR shows an essential role in caPSCs activation and caPSCs-induced PCCs aggressiveness in our project. Here we will make a detailed discussion based on our results and published literature.

4.1. Isolation and verification of human PSCs

First, efficient PSCs isolation and verification methods are certainly important for deeply researching PSCs' role in PDAC and CP. Although immortalized PSCs were reported[133, 136], primary PSCs are still the main research tools [8]. As reported by the Pancreatic Star Alliance, M. Buchholz found that a single injection of immortalized PSCs to nude mice sometimes resulted in invasive anaplastic PDAC, demonstrating that immortalization technologies require improvement[8]. Although isolation methods for murine primary PSCs were developed in 1998 and very mature, literature also indicated that species variances exist between murine and human PSCs[8, 137]. Therefore, we used human primary PSCs, both activated and quiescent, in our research. The outgrowth method for human caPSCs and cpPSCs was invented in 1998[39], while the density centrifugation method for human quiescent PSCs (nPSCs) was not developed until 2010[119]. Based on their great work on both methods, we further improved the isolation methods according to our practices and successfully established caPSCs, cpPSCs, and nPSCs in our lab. For the caPSCs and cpPSCs, we made improvement as follows: a) tissues were removed of adipose, connective section as well as blood before further processing because theses would lead to cell contaminations; b) the entire isolation process should be as soon as possible because cells would be dead after tissues were resected; c) due to the previous trimming process, the culture procedure after seeding was simplified to a daily refreshment of

medium but not the complex refreshment-reseeding procedure. As to the outcomes, emerging timepoint from tissue blocks, Bachem et al. reported a 3-5 days after seeding for cpPSCs[39], and we showed the same results in both cpPSCs and caPSCs with an over 90% viability. A similar result was also achieved: nPSCs could not grow out from normal pancreas tissue block using the outgrowth method[39]. Morphologically, the activated PSCs showed a star-shaped with no lipid droplets inside, consistent with the previous descriptions[37, 39]. For the density centrifugation method, a) the injection procedure[119] was omitted, and single 15-minute digestion in a shaking water bath accelerated the digestion procedure; b) 2.5μg/mL AmB was applied in the complete medium to avoid potential fungal contamination. Vonlaufen et al reported 0.2-1.4x10^6/g (n=5), and we have a similar yield of 0.3-1.6x10^6/g human nPSCs (n=5) with over 90% viability (Figure 3B, Table 3). Compared to the yield of rat nPSCs (about 3x106/g), human nPSCs have a relatively lower yield due to the higher proportion of fat, connective, and vascular tissues in the human pancreas. As to the morphology of human nPSCs, both the two published papers[119, 138] and we indicated that freshly separated human nPSCs indicated an irregular shape with abundant perinuclear lipid droplets, and following treatment with trypsin for the 1st passage, all nPSCs transformed into the activated phenotype, which lost lipid droplets and showed a stellate-like shape. In the verification of human PSCs, ICC staining of αSMA and desmin was utilized. ICC showed a 100% αSMA and 40-55% desmin staining, which were similar to the data from Bachem[39] (αSMA: >90% positive, desmin: 20%-50% positive), Tian[138] (αSMA: strong positive, desmin: partly positive) and Qian[60] (αSMA: positive, desmin: positive) on human PSCs[39]. This indicated that the human primary nPSCs, caPSCs, and cpPSCs were successfully established in our lab.

In conclusion, based on other scientists' outstanding work and our practices, the improved isolation methods in our lab have the advantage of more simplified steps without affecting the efficiency of PSCs separation.

4.2. VDR in PSCs activation process

Four studies are found in investigating the effect of VDR ligand on PSCs activation[79, 120, 121, 139]. This section will discuss our results and the published data to better understand VDR's role in PSCs activation.

To begin with, we checked the VDR expression and activity in caPSCs and PCCs and found that caPSCs exhibited a relatively higher expression of VDR and activity than PCCs. This finding is consistent with the previous data[79], both of which indicated that VDR is a promising druggable receptor in caPSCs.

Then we conducted ICC, WB, and qRT-PCR to explore the effects of VDR ligand upon caPSCs with αSMA as the indicator of activation. Our ICC result showed that αSMA staining in caPSCs incubated with Cal significantly is stronger than the control group, which indicated an inhibitory effect of VDR ligand on activation of caPSCs. WB and qRT-PCR exhibited similar results in that VDR increased, whereas those of αSMA decreased after caPSCs were treated with VDR ligand. Sherman et al. showed that αSMA mRNA decreased and lipid droplets (the feature of quiescent PSCs) reformated after VDR ligand treatment[79]. Our findings, both at protein and mRNA levels, further confirmed the hypothesis that VDR induction by its ligand opposed the activation procedure of caPSCs.

Additionally, we assessed this effect in cpPSCs and nPSCs (culture-activated) and further investigated the correlation between VDR and αSMA at the mRNA level. qRT-PCR revealed that VDR mRNA increased whereas αSMA mRNA decreased in the two kinds of PSCs treated with VDR ligand compared to the control group. Unlike our study using human PSCs, cpPSCs and culture-activated nPSCs in the published papers were all from murine sources [121, 139]. Wallbaum et al. indicated that the VDR ligand

reduced αSMA protein expression and prevented lipids loss in culture-activated murine nPSCs[139]. Kang et al. demonstrated that VDR ligand impeded αSMA expression using ICC assay in the CP mouse model[121]. All studies from human PSCs and murine showed that the VDR ligand diminished the PSCs activation. Moreover, we first reported that VDR was in a moderate negative correlation with αSMA expression using qRT-PCR, which further proved a critical role of VDR in the PSCs activation process. In addition, we first comprehensively investigated VDR's effects on the activation of all three kinds of PSCs with human sources.

Migration ability is a feature of activated PSCs, which enable PSCs to accumulate in disease regions[126-130]. caPSCs showed the ability of migration when exposed to cancer cell secretions[6]. No papers about the effects of VDR ligand upon caPSCs migration were published after literature searching. Therefore, we conducted a transwell migration experiment and WH test and found that the VDR ligand significantly decreased the migration ability of activated caPSCs. We explain that the VDR ligand diminishes the autocrine secretion of caPSCs which keeps themselves activated and enables them to migrate.

As another feature of activated PSCs, proliferation ability combined with migration ability contributes to increased PSCs in diseases like CP and PDAC[8, 9, 131, 132]. EZ4U assay demonstrated that the VDR ligand reduced the proliferation ability of caPSCs, but not that of freshly isolated nPSCs. Blauer demonstrated that $1,25(OH)_2D_3$ reduced the proliferation ability of culture-activated murine PSCs by colorimetric crystal violet assay. However, Wallbaum reported that VDR ligands have no effect on murine culture-activated nPSCs by BrdU assay. The possible reason for this difference might be PSCs with different sources, different monitoring methods, and different drug treatment time.

Overall, VDR plays a significant role in PSCs activation, migration, and proliferation. VDR ligand is expected to become a powerful tool to prevent the severe desmoplasia reaction of PDAC and improve PDAC therapy.

4.3. VDR in caPSCs-augmented aggressiveness of PCCs

Previous works have indicated that caPSCs release various molecules, enhancing the aggressiveness (e.g., migration, invasion, proliferation) of PCCs[51, 55, 92, 134, 140-144]. Targeting the paracrine crosstalk has become hotspots in researches on anti-PSCs strategy recently. However, little evidence was found about the effects of VDR ligand on caPSCs-PCCs crosstalk.

Since the VDR ligand could inhibit the caPSCs activation, we hypothesized that caPSCs deactivated by the VDR ligand released fewer molecules, leading to less aggressiveness of PCCs. Therefore, we cocultured three caPSCs and three PCCs in the transwell system and found that both migration and invasion abilities of PCCs were impeded when cocultured with deactivated caPSCs. We explain that the VDR ligand inhibits caPSCs activation as well as reducing tumorigenic molecule secretion.

We then assessed the proliferation ability of three PCCs using CM from three caPSCs, respectively. EZ4U showed that CM from caPSCs deactivated by VDR ligand significantly decreased the proliferation ability of all three PCCs. Results showed that VDR activation in caPSCs negatively regulated the caPSCs-augmented proliferation of PCCs. The paracrine molecules, which promote PCCs proliferation, might be inhibited by VDR ligand in caPSCs

In summary, we indicated the VDR ligand as a potential target to reduce the caPSCs-enhanced aggressive behavior of PCCs.

4.4. Conclusion and Outlook

In conclusion, VDR activation by its ligand deactivated caPSCs and then diminished caPSCs-enhanced PDAC aggressiveness. Our work indicated that VDR is a potential anti-stroma method for PDAC therapy.

In future work, we are going to explore the deep mechanism further. This may include but is not limited to: a) identify the potential molecules influenced by VDR ligand and play a role in the caPSCs-PCCs crosstalk. b) the mechanisms by which these caPSCs-secreted molecules influence the aggressiveness of PCCs and how the VDR ligand will attenuate this effect. c) further verification in an animal model or PDAC organoid model. d) the correlation between these molecules and clinical data of PDAC.

5. Summary

The dismal prognosis of PDAC owns to a pro-tumorigenic stroma which occupies most (50%-80%) of tumor volume and increases chemoresistance. PSCs transformation from quiescent to activated phenotype is the leading cause of the severe stromal reaction. Since standard chemotherapy has displayed disappointing outcomes, stroma targeting strategy and chemotherapy have become the research hotspot. VDR has been well investigated in hepatic fibrosis caused by activated HSCs and emerged as a promising anti-stroma target in PDAC therapy. This project is devoted to exploring the role of VDR on PSCs deactivation and caPSCs-PCCs crosstalk in vitro, which would provide an anti-stromal target for PDAC treatment.

The technique to isolate both the quiescent PSCs from the normal pancreas and the activated PSCs from tumor tissue of patients suffering from PDAC or chronic pancreatitis was established and verified by ICC. VDR was revealed to be highly expressed in caPSCs as opposed to PCCs. VDR induction by calcipotriol, a vitamin D analog, markedly reduced caPSCs activation markers at mRNA and protein levels. This decreased caPSCs activation by VDR induction through calcipotriol diminished the proliferation of caPSCs. In addition, caPSCs migration was also reduced after VDR stimulation in both WH assay and transwell migration assays. In the caPSCs-PCCs co-culture system, VDR activation in caPSCs significantly reduced caPSCs-augmented progression of pancreatic tumor cells, including migration, invasion, and proliferation utilizing transwell migration, invasion, and EZ4U assay, respectively.

In conclusion, VDR induction by its ligand deactivated caPSCs and reduced caPSCs-augmented PDAC progression. This work suggested VDR as a promising target for stromal reprogramming and PDAC therapy.

6. Zusammenfassung

Das Pankreaskarzinom ist durch eine ausgeprägte stromale Beteiligung gekennzeichnet bei dem der stromalen Anteil in der Regel die Mehrheit (50-80%) des Tumorvolumens ausmacht. Aktivierte pankreatische Stellatumzellen (PSCs) spielen eine entscheidende Rolle bei der Fibrogenese und stimulieren das Tumorzellwachstum. Nachdem konventionelle Chemotherapeutika beim Pankreaskarzinom bisher eher enttäuschende Ergebnisse gezeigt haben, ist nun die Frage entstanden ob nicht durch eine zusätzliche Modifikation des Stromas bessere anti-tumorale Wirkungen erzielt werden können. Der Vitamin-D Rezeptor VDR ist bei aktivierten hepatischen Sternzellen und der Leberfibrose gut untersucht und stellt auch in der anti-stromalen Therapie beim Pankreaskarzinom ein vielversprechendes Ziel dar.

In dieser Arbeit wurde zunächst die Isolation von primären Stellatumzellen (sowohl aktivierte als auch Ruhe-PSCs) aus Geweben von Patienten mit Pankreaskarzinom oder chronischer Pankreatitis etabliert und mittels der Immunzytologie weiter verifiziert. Hierbei fiel auf, dass der Vitamin-D Rezeptor VDR in PSCs, also im Stroma von Patienten mit Pankreaskarzinom höher exprimiert werden als in den primären Tumorzellen. Eine VDR Stimulation durch das potente Vitamin D Analogon Calcipotriol reduzierte den Aktivierungszustand dieser PSCs deutlich. Diese stimulierten, und damit weniger aktivierten PSCs zeigten funktionell auch eine deutlich verminderte Migration und Proliferation. Darüber hinaus zeigte sich in der Co-Kultur eine signifikant verminderte Proliferation, Migration und Invasion der Pankreaskarzinomzellen, wenn Sie mit Calcipotriol vorbehandelten PSCs co-kultiviert wurden.

Zusammenfassend konnte in der vorliegenden Arbeit gezeigt werden, dass eine Behandlung von pankreatischen Stellatumzellen mit einem Vitamin D Analogon zu

weniger aktivierten PSCs und somit indirekt zu einem weniger aggressiven Verhalten der Pankreaskarzinomzellen in vitro führt. Der Vitamin D Rezeptor VDR stellt somit ein vielversprechendes Ziel für eine anti-tumorale Modifikation des Stromas beim Pankreaskarzinom dar.

III. Reference

1. Siegel, R.L., K.D. Miller, and A. Jemal, *Cancer statistics, 2019.* CA Cancer J Clin, 2019. **69**(1): p. 7-34.

2. McGuigan, A., et al., *Pancreatic cancer: A review of clinical diagnosis, epidemiology, treatment and outcomes.* World J Gastroenterol, 2018. **24**(43): p. 4846-4861.

3. Rawla, P., T. Sunkara, and V. Gaduputi, *Epidemiology of Pancreatic Cancer: Global Trends, Etiology and Risk Factors.* World J Oncol, 2019. **10**(1): p. 10-27.

4. McGuire, S., *World Cancer Report 2014. Geneva, Switzerland: World Health Organization, International Agency for Research on Cancer, WHO Press, 2015.* Adv Nutr, 2016. **7**(2): p. 418-9.

5. Tempero, M.A., et al., *Pancreatic Adenocarcinoma, Version 1.2019.* J Natl Compr Canc Netw, 2019. **17**(3): p. 202-210.

6. Apte, M.V., et al., *Desmoplastic reaction in pancreatic cancer - Role of pancreatic stellate cells.* Pancreas, 2004. **29**(3): p. 179-187.

7. Vonlaufen, A., et al., *Pancreatic stellate cells and pancreatic cancer cells: An unholy alliance.* Cancer Research, 2008. **68**(19): p. 7707-7710.

8. Erkan, M., et al., *StellaTUM: current consensus and discussion on pancreatic stellate cell research.* Gut, 2012. **61**(2): p. 172-178.

9. Apte, M.V., et al., *A Starring Role for Stellate Cells in the Pancreatic Cancer Microenvironment.* Gastroenterology, 2013. **144**(6): p. 1210-1219.

10. Tzilas, V., et al., *Vitamin D prevents experimental lung fibrosis and predicts survival in patients with idiopathic pulmonary fibrosis.* Pulm Pharmacol Ther, 2019. **55**: p. 17-24.

11. He, X., et al., *MicroRNA-351 promotes schistosomiasis-induced hepatic*

fibrosis by targeting the vitamin D receptor. Proc Natl Acad Sci U S A, 2018. **115**(1): p. 180-185.

12. Duran, A., et al., *p62/SQSTM1 by Binding to Vitamin D Receptor Inhibits Hepatic Stellate Cell Activity, Fibrosis, and Liver Cancer.* Cancer Cell, 2016. **30**(4): p. 595-609.

13. Tian, Y., et al., *Effects of vitamin D on renal fibrosis in diabetic nephropathy model rats.* Int J Clin Exp Pathol, 2014. **7**(6): p. 3028-37.

14. Ding, N., et al., *A vitamin D receptor/SMAD genomic circuit gates hepatic fibrotic response.* Cell, 2013. **153**(3): p. 601-13.

15. Bray, F., et al., *Global cancer statistics 2018: GLOBOCAN estimates of incidence and mortality worldwide for 36 cancers in 185 countries.* CA Cancer J Clin, 2018. **68**(6): p. 394-424.

16. Ferlay J, E.M., Lam F, Colombet M, Mery L, Piñeros M, Znaor A, Soerjomataram I, Bray F. *Global cancer observatory: cancer today*. 2018.

17. Bosetti, C., et al., *Cigarette smoking and pancreatic cancer: an analysis from the International Pancreatic Cancer Case-Control Consortium (Panc4).* Ann Oncol, 2012. **23**(7): p. 1880-8.

18. Klein, A.P., et al., *Prospective risk of pancreatic cancer in familial pancreatic cancer kindreds.* Cancer Res, 2004. **64**(7): p. 2634-8.

19. Chu, G.C., et al., *Stromal biology of pancreatic cancer.* J Cell Biochem, 2007. **101**(4): p. 887-907.

20. Vennin, C., et al., *Reshaping the Tumor Stroma for Treatment of Pancreatic Cancer.* Gastroenterology, 2018. **154**(4): p. 820-838.

21. Neesse, A., et al., *Stromal biology and therapy in pancreatic cancer: ready for clinical translation?* Gut, 2019. **68**(1): p. 159-171.

22. Kong, X., et al., *Targeted destruction of the orchestration of the pancreatic stroma and tumor cells in pancreatic cancer cases: molecular basis for therapeutic implications.* Cytokine Growth Factor Rev, 2012. **23**(6): p. 343-56.

23. Feig, C., et al., *The Pancreas Cancer Microenvironment.* Clinical Cancer

Research, 2012. **18**(16): p. 4266-4276.

24. Farran, B. and G.P. Nagaraju, *The dynamic interactions between the stroma, pancreatic stellate cells and pancreatic tumor development: Novel therapeutic targets.* Cytokine Growth Factor Rev, 2019. **48**: p. 11-23.

25. Xiao, Y., et al., *YAP1-mediated pancreatic stellate cell activation inhibits pancreatic cancer cell proliferation.* Cancer Lett, 2019. **462**: p. 51-60.

26. Horioka, K., et al., *Suppression of CD51 in pancreatic stellate cells inhibits tumor growth by reducing stroma and altering tumor-stromal interaction in pancreatic cancer.* Int J Oncol, 2016. **48**(4): p. 1499-508.

27. Dalin, S., et al., *Deoxycytidine Release from Pancreatic Stellate Cells Promotes Gemcitabine Resistance.* Cancer Res, 2019. **79**(22): p. 5723-5733.

28. Wen, Z., et al., *Fibroblast activation protein alpha-positive pancreatic stellate cells promote the migration and invasion of pancreatic cancer by CXCL1-mediated Akt phosphorylation.* Ann Transl Med, 2019. **7**(20): p. 532.

29. Kuninty, P.R., et al., *ITGA5 inhibition in pancreatic stellate cells attenuates desmoplasia and potentiates efficacy of chemotherapy in pancreatic cancer.* Sci Adv, 2019. **5**(9): p. eaax2770.

30. Yuan, Y., et al., *BAG3-positive pancreatic stellate cells promote migration and invasion of pancreatic ductal adenocarcinoma.* J Cell Mol Med, 2019. **23**(8): p. 5006-5016.

31. Junliang, L., et al., *High-molecular-weight hyaluronan produced by activated pancreatic stellate cells promotes pancreatic cancer cell migration via paracrine signaling.* Biochem Biophys Res Commun, 2019. **515**(3): p. 493-498.

32. Hwang, H.J., et al., *Multiplex quantitative analysis of stroma-mediated cancer cell invasion, matrix remodeling, and drug response in a 3D co-culture model of pancreatic tumor spheroids and stellate cells.* J Exp Clin Cancer Res, 2019. **38**(1): p. 258.

33. Wang, H.C., et al., *Pancreatic stellate cells activated by mutant KRAS-mediated PAI-1 upregulation foster pancreatic cancer progression via IL-8.* Theranostics, 2019. **9**(24): p. 7168-7183.

34. Nan, L., et al., *Pancreatic Stellate Cells Facilitate Perineural Invasion of Pancreatic Cancer via HGF/c-Met Pathway.* Cell Transplant, 2019. **28**(9-10): p. 1289-1298.

35. Tang, D., et al., *Identification of key pathways and gene changes in primary pancreatic stellate cells after cross-talk with pancreatic cancer cells (BXPC-3) using bioinformatics analysis.* Neoplasma, 2019. **66**(3): p. 446-458.

36. Zhou, L., et al., *Suppression of stromal-derived Dickkopf-3 (DKK3) inhibits tumor progression and prolongs survival in pancreatic ductal adenocarcinoma.* Sci Transl Med, 2018. **10**(464).

37. Watari, N., Y. Hotta, and Y. Mabuchi, *Morphological studies on a vitamin A-storing cell and its complex with macrophage observed in mouse pancreatic tissues following excess vitamin A administration.* Okajimas Folia Anat Jpn, 1982. **58**(4-6): p. 837-58.

38. Apte, M.V., et al., *Periacinar stellate shaped cells in rat pancreas: identification, isolation, and culture.* Gut, 1998. **43**(1): p. 128-133.

39. Bachem, M.G., et al., *Identification, culture, and characterization of pancreatic stellate cells in rats and humans.* Gastroenterology, 1998. **115**(2): p. 421-432.

40. Apte, M.V. and J.S. Wilson, *Mechanisms of pancreatic fibrosis.* Digestive Diseases, 2004. **22**(3): p. 273-279.

41. Mews, P., et al., *Pancreatic stellate cells respond to inflammatory cytokines: potential role in chronic pancreatitis.* Gut, 2002. **50**(4): p. 535-541.

42. Haber, P.S., et al., *Activation of pancreatic stellate cells in human and experimental pancreatic fibrosis.* American Journal of Pathology, 1999. **155**(4): p. 1087-1095.

43. Bynigeri, R.R., et al., *Pancreatic stellate cell: Pandora's box for pancreatic disease biology.* World Journal of Gastroenterology, 2017. **23**(3): p. 382-405.

44. Apte, M.V., et al., *Pancreatic stellate cells are activated by proinflammatory cytokines: implications for pancreatic fibrogenesis.* Gut, 1999. **44**(4): p. 534-541.

45. McCarroll, J.A., et al., *Role of pancreatic stellate cells in chemoresistance in*

pancreatic cancer. Front Physiol, 2014. **5**: p. 141.

46. Berchtold, S., et al., *Collagen type V promotes the malignant phenotype of pancreatic ductal adenocarcinoma.* Cancer Lett, 2015. **356**(2 Pt B): p. 721-32.

47. Di Maggio, F., et al., *Pancreatic stellate cells regulate blood vessel density in the stroma of pancreatic ductal adenocarcinoma.* Pancreatology, 2016. **16**(6): p. 995-1004.

48. Provenzano, P.P., et al., *Enzymatic targeting of the stroma ablates physical barriers to treatment of pancreatic ductal adenocarcinoma.* Cancer Cell, 2012. **21**(3): p. 418-29.

49. Schnittert, J., R. Bansal, and J. Prakash, *Targeting Pancreatic Stellate Cells in Cancer.* Trends Cancer, 2019. **5**(2): p. 128-142.

50. Halbrook, C.J. and C.A. Lyssiotis, *Employing Metabolism to Improve the Diagnosis and Treatment of Pancreatic Cancer.* Cancer Cell, 2017. **31**(1): p. 5-19.

51. Sousa, C.M., et al., *Pancreatic stellate cells support tumour metabolism through autophagic alanine secretion.* Nature, 2016. **536**(7617): p. 479-83.

52. Zhao, H., et al., *Tumor microenvironment derived exosomes pleiotropically modulate cancer cell metabolism.* Elife, 2016. **5**: p. e10250.

53. Cao, F., et al., *HES 1 is essential for chemoresistance induced by stellate cells and is associated with poor prognosis in pancreatic cancer.* Oncol Rep, 2015. **33**(4): p. 1883-9.

54. Liu, Y., et al., *Periostin promotes the chemotherapy resistance to gemcitabine in pancreatic cancer.* Tumour Biol, 2016. **37**(11): p. 15283-15291.

55. Zhang, H., et al., *Paracrine SDF-1alpha signaling mediates the effects of PSCs on GEM chemoresistance through an IL-6 autocrine loop in pancreatic cancer cells.* Oncotarget, 2015. **6**(5): p. 3085-97.

56. Amrutkar, M., et al., *Secretion of fibronectin by human pancreatic stellate cells promotes chemoresistance to gemcitabine in pancreatic cancer cells.* BMC Cancer, 2019. **19**(1): p. 596.

57. Tang, D., et al., *Persistent activation of pancreatic stellate cells creates a microenvironment favorable for the malignant behavior of pancreatic ductal adenocarcinoma.* Int J Cancer, 2013. **132**(5): p. 993-1003.

58. Schnittert, J., et al., *Integrin alpha11 in pancreatic stellate cells regulates tumor stroma interaction in pancreatic cancer.* FASEB J, 2019. **33**(5): p. 6609-6621.

59. Kikuta, K., et al., *Pancreatic stellate cells promote epithelial-mesenchymal transition in pancreatic cancer cells.* Biochemical and Biophysical Research Communications, 2010. **403**(3-4): p. 380-384.

60. Qian, D., et al., *Galectin-1-driven upregulation of SDF-1 in pancreatic stellate cells promotes pancreatic cancer metastasis.* Cancer Lett, 2017. **397**: p. 43-51.

61. Tang, D., et al., *High expression of Galectin-1 in pancreatic stellate cells plays a role in the development and maintenance of an immunosuppressive microenvironment in pancreatic cancer.* Int J Cancer, 2012. **130**(10): p. 2337-48.

62. Incio, J., et al., *Obesity-Induced Inflammation and Desmoplasia Promote Pancreatic Cancer Progression and Resistance to Chemotherapy.* Cancer Discov, 2016. **6**(8): p. 852-69.

63. Gabitass, R.F., et al., *Elevated myeloid-derived suppressor cells in pancreatic, esophageal and gastric cancer are an independent prognostic factor and are associated with significant elevation of the Th2 cytokine interleukin-13.* Cancer Immunol Immunother, 2011. **60**(10): p. 1419-30.

64. Markowitz, J., et al., *Patients with pancreatic adenocarcinoma exhibit elevated levels of myeloid-derived suppressor cells upon progression of disease.* Cancer Immunol Immunother, 2015. **64**(2): p. 149-59.

65. Wu, Q., et al., *Functions of pancreatic stellate cell-derived soluble factors in the microenvironment of pancreatic ductal carcinoma.* Oncotarget, 2017. **8**(60): p. 102721-102738.

66. Mace, T.A., M. Bloomston, and G.B. Lesinski, *Pancreatic cancer-associated stellate cells: A viable target for reducing immunosuppression in the tumor microenvironment.* Oncoimmunology, 2013. **2**(7): p. e24891.

67. Ene-Obong, A., et al., *Activated pancreatic stellate cells sequester CD8+ T*

cells to reduce their infiltration of the juxtatumoral compartment of pancreatic ductal adenocarcinoma. Gastroenterology, 2013. **145**(5): p. 1121-32.

68. Kuninty, P.R., et al., *MicroRNA-199a and -214 as potential therapeutic targets in pancreatic stellate cells in pancreatic tumor.* Oncotarget, 2016. **7**(13): p. 16396-408.

69. Whatcott, C.J., et al., *Inhibition of ROCK1 kinase modulates both tumor cells and stromal fibroblasts in pancreatic cancer.* PLoS One, 2017. **12**(8): p. e0183871.

70. Zhang, Y., et al., *Vitamin A-coupled liposomes carrying TLR4-silencing shRNA induce apoptosis of pancreatic stellate cells and resolution of pancreatic fibrosis.* J Mol Med (Berl), 2018. **96**(5): p. 445-458.

71. Yeo, D., et al., *Inhibition of group 1 p21-activated kinases suppresses pancreatic stellate cell activation and increases survival of mice with pancreatic cancer.* Int J Cancer, 2017. **140**(9): p. 2101-2111.

72. Han, L., et al., *Pancreatic stellate cells contribute pancreatic cancer pain via activation of sHH signaling pathway.* Oncotarget, 2016. **7**(14): p. 18146-58.

73. Olive, K.P., et al., *Inhibition of Hedgehog signaling enhances delivery of chemotherapy in a mouse model of pancreatic cancer.* Science, 2009. **324**(5933): p. 1457-61.

74. Rhim, A.D., et al., *Stromal Elements Act to Restrain, Rather Than Support, Pancreatic Ductal Adenocarcinoma.* Cancer Cell, 2014. **25**(6): p. 735-747.

75. Amakye, D., Z. Jagani, and M. Dorsch, *Unraveling the therapeutic potential of the Hedgehog pathway in cancer.* Nat Med, 2013. **19**(11): p. 1410-22.

76. Ozdemir, B.C., et al., *Depletion of Carcinoma-Associated Fibroblasts and Fibrosis Induces Immunosuppression and Accelerates Pancreas Cancer with Reduced Survival.* Cancer Cell, 2015. **28**(6): p. 831-833.

77. Prakash, J., *Cancer-Associated Fibroblasts: Perspectives in Cancer Therapy.* Trends Cancer, 2016. **2**(6): p. 277-279.

78. Schnittert, J., et al., *Reprogramming tumor stroma using an endogenous lipid lipoxin A4 to treat pancreatic cancer.* Cancer Lett, 2018. **420**: p. 247-258.

79. Sherman, M.H., et al., *Vitamin D Receptor-Mediated Stromal Reprogramming Suppresses Pancreatitis and Enhances Pancreatic Cancer Therapy.* Cell, 2014. **159**(1): p. 80-93.

80. Froeling, F.E.M., et al., *Retinoic Acid-Induced Pancreatic Stellate Cell Quiescence Reduces Paracrine Wnt-beta-Catenin Signaling to Slow Tumor Progression.* Gastroenterology, 2011. **141**(4): p. 1486-U503.

81. Kota, J., et al., *Pancreatic cancer: Stroma and its current and emerging targeted therapies.* Cancer Lett, 2017. **391**: p. 38-49.

82. Jaster, R., et al., *Regulation of pancreatic stellate cell function in vitro: biological and molecular effects of all-trans retinoic acid.* Biochem Pharmacol, 2003. **66**(4): p. 633-41.

83. McCarroll, J.A., et al., *Vitamin A inhibits pancreatic stellate cell activation: implications for treatment of pancreatic fibrosis.* Gut, 2006. **55**(1): p. 79-89.

84. Han, X., et al., *Reversal of pancreatic desmoplasia by re-educating stellate cells with a tumour microenvironment-activated nanosystem.* Nat Commun, 2018. **9**(1): p. 3390.

85. Michael, A., et al., *13-cis-Retinoic acid in combination with gemcitabine in the treatment of locally advanced and metastatic pancreatic cancer--report of a pilot phase II study.* Clin Oncol (R Coll Radiol), 2007. **19**(2): p. 150-3.

86. Moore, D.F., Jr., et al., *Pilot phase II trial of 13-cis-retinoic acid and interferon-alpha combination therapy for advanced pancreatic adenocarcinoma.* Am J Clin Oncol, 1995. **18**(6): p. 525-7.

87. Kozono, S., et al., *Pirfenidone inhibits pancreatic cancer desmoplasia by regulating stellate cells.* Cancer Res, 2013. **73**(7): p. 2345-56.

88. Suklabaidya, S., et al., *Characterization and use of HapT1-derived homologous tumors as a preclinical model to evaluate therapeutic efficacy of drugs against pancreatic tumor desmoplasia.* Oncotarget, 2016. **7**(27): p. 41825-41842.

89. Kuninty, P.R., et al., *MicroRNA Targeting to Modulate Tumor Microenvironment.* Front Oncol, 2016. **6**: p. 3.

90. Kwon, J.J., et al., *Pathophysiological role of microRNA-29 in pancreatic cancer*

stroma. Sci Rep, 2015. **5**: p. 11450.

91. Asama, H., et al., *MicroRNA let-7d targets thrombospondin-1 and inhibits the activation of human pancreatic stellate cells.* Pancreatology, 2019. **19**(1): p. 196-203.

92. Orozco, C.A., et al., *Targeting galectin-1 inhibits pancreatic cancer progression by modulating tumor-stroma crosstalk.* Proc Natl Acad Sci U S A, 2018. **115**(16): p. E3769-E3778.

93. Jacobetz, M.A., et al., *Hyaluronan impairs vascular function and drug delivery in a mouse model of pancreatic cancer.* Gut, 2013. **62**(1): p. 112-20.

94. Hingorani, S.R., et al., *Phase Ib Study of PEGylated Recombinant Human Hyaluronidase and Gemcitabine in Patients with Advanced Pancreatic Cancer.* Clin Cancer Res, 2016. **22**(12): p. 2848-54.

95. Hingorani, S.R., et al., *HALO 202: Randomized Phase II Study of PEGPH20 Plus Nab-Paclitaxel/Gemcitabine Versus Nab-Paclitaxel/Gemcitabine in Patients With Untreated, Metastatic Pancreatic Ductal Adenocarcinoma.* J Clin Oncol, 2018. **36**(4): p. 359-366.

96. Masamune, A., et al., *The angiotensin II type I receptor blocker olmesartan inhibits the growth of pancreatic cancer by targeting stellate cell activities in mice.* Scand J Gastroenterol, 2013. **48**(5): p. 602-9.

97. Chauhan, V.P., et al., *Angiotensin inhibition enhances drug delivery and potentiates chemotherapy by decompressing tumour blood vessels.* Nat Commun, 2013. **4**: p. 2516.

98. Bramhall, S.R., et al., *A double-blind placebo-controlled, randomised study comparing gemcitabine and marimastat with gemcitabine and placebo as first line therapy in patients with advanced pancreatic cancer.* Br J Cancer, 2002. **87**(2): p. 161-7.

99. Kocher, H., et al., *STAR_PAC: A Phase 1B study repurposing ATRA as stromal targeting agent along with gemcitabine and nab¬Paclitaxel for pancreatic cancer.* Pancreatology, 2016. **16**(3, Supplement): p. S4-S5.

100. Banerjee, S., et al., *Impaired Synthesis of Stromal Components in Response to Minnelide Improves Vascular Function, Drug Delivery, and Survival in*

Pancreatic Cancer. Clin Cancer Res, 2016. **22**(2): p. 415-25.

101. Kumar, K., et al., *BET inhibitors block pancreatic stellate cell collagen I production and attenuate fibrosis in vivo.* JCI Insight, 2017. **2**(3): p. e88032.

102. Steele, C.W., et al., *CXCR2 Inhibition Profoundly Suppresses Metastases and Augments Immunotherapy in Pancreatic Ductal Adenocarcinoma.* Cancer Cell, 2016. **29**(6): p. 832-845.

103. Feig, C., et al., *Targeting CXCL12 from FAP-expressing carcinoma-associated fibroblasts synergizes with anti-PD-L1 immunotherapy in pancreatic cancer.* Proc Natl Acad Sci U S A, 2013. **110**(50): p. 20212-7.

104. Tao, Q., et al., *Vitamin D prevents the intestinal fibrosis via induction of vitamin D receptor and inhibition of transforming growth factor-beta1/Smad3 pathway.* Dig Dis Sci, 2015. **60**(4): p. 868-75.

105. Pattanaik, D., et al., *Pathogenesis of Systemic Sclerosis.* Front Immunol, 2015. **6**: p. 272.

106. Potter, J.J., et al., *1,25-dihydroxyvitamin D3 and its nuclear receptor repress human alpha1 (I) collagen expression and type I collagen formation.* Liver Int, 2013. **33**(5): p. 677-86.

107. Lichtler, A., et al., *Isolation and characterization of the rat alpha 1(I) collagen promoter. Regulation by vitamin D.* J Biol Chem, 1994. **269**(23): p. 16518.

108. Puche, J.E., Y. Saiman, and S.L. Friedman, *Hepatic stellate cells and liver fibrosis.* Compr Physiol, 2013. **3**(4): p. 1473-92.

109. Hellerbrand, C., *Hepatic stellate cells--the pericytes in the liver.* Pflugers Arch, 2013. **465**(6): p. 775-8.

110. Abramovitch, S., et al., *Vitamin D inhibits proliferation and profibrotic marker expression in hepatic stellate cells and decreases thioacetamide-induced liver fibrosis in rats.* Gut, 2011. **60**(12): p. 1728-37.

111. Zerr, P., et al., *Vitamin D receptor regulates TGF-beta signalling in systemic sclerosis.* Ann Rheum Dis, 2015. **74**(3): p. e20.

112. Meredith, A., et al., *1,25 Dihydroxyvitamin D3 Inhibits TGFbeta1-Mediated*

Primary Human Cardiac Myofibroblast Activation. PLoS One, 2015. **10**(6): p. e0128655.

113. Mokady, E., et al., *A protective role of dietary vitamin D3 in rat colon carcinogenesis.* Nutr Cancer, 2000. **38**(1): p. 65-73.

114. Mohr, S.B., et al., *Could vitamin D sufficiency improve the survival of colorectal cancer patients?* J Steroid Biochem Mol Biol, 2015. **148**: p. 239-44.

115. Klampfer, L., *Vitamin D and colon cancer.* World J Gastrointest Oncol, 2014. **6**(11): p. 430-7.

116. Pereira, F., M.J. Larriba, and A. Munoz, *Vitamin D and colon cancer.* Endocr Relat Cancer, 2012. **19**(3): p. R51-71.

117. Ferrer-Mayorga, G., et al., *Vitamin D receptor expression and associated gene signature in tumour stromal fibroblasts predict clinical outcome in colorectal cancer.* Gut, 2017. **66**(8): p. 1449-1462.

118. Kong, F., et al., *VDR signaling inhibits cancer-associated-fibroblasts' release of exosomal miR-10a-5p and limits their supportive effects on pancreatic cancer cells.* Gut, 2019. **68**(5): p. 950-951.

119. Vonlaufen, A., et al., *Isolation of quiescent human pancreatic stellate cells: a promising in vitro tool for studies of human pancreatic stellate cell biology.* Pancreatology, 2010. **10**(4): p. 434-43.

120. Blauer, M., J. Sand, and J. Laukkarinen, *Physiological and clinically attainable concentrations of 1,25-dihydroxyvitamin D3 suppress proliferation and extracellular matrix protein expression in mouse pancreatic stellate cells.* Pancreatology, 2015. **15**(4): p. 366-71.

121. Kang, Z.S., et al., *Design, synthesis and biological evaluation of non-secosteriodal vitamin D receptor ligand bearing double side chain for the treatment of chronic pancreatitis.* Eur J Med Chem, 2018. **146**: p. 541-553.

122. Jones, G., D.E. Prosser, and M. Kaufmann, *Cytochrome P450-mediated metabolism of vitamin D.* J Lipid Res, 2014. **55**(1): p. 13-31.

123. Ramirez, A.M., et al., *Vitamin D inhibition of pro-fibrotic effects of transforming growth factor beta1 in lung fibroblasts and epithelial cells.* J Steroid Biochem

Mol Biol, 2010. **118**(3): p. 142-50.

124. Ito, I., et al., *A nonclassical vitamin D receptor pathway suppresses renal fibrosis.* J Clin Invest, 2013. **123**(11): p. 4579-94.

125. Zhang, Y., et al., *Vitamin D receptor attenuates renal fibrosis by suppressing the renin-angiotensin system.* J Am Soc Nephrol, 2010. **21**(6): p. 966-73.

126. Phillips, P.A., et al., *Cell migration: a novel aspect of pancreatic stellate cell biology.* Gut, 2003. **52**(5): p. 677-682.

127. Rosendahl, A.H., et al., *Conditionally immortalized human pancreatic stellate cell lines demonstrate enhanced proliferation and migration in response to IGF-I.* Exp Cell Res, 2015. **330**(2): p. 300-10.

128. Tian, L., et al., *Activation of pancreatic stellate cells involves an EMT-like process.* Int J Oncol, 2016. **48**(2): p. 783-92.

129. Ben-Harosh, Y., et al., *Pancreatic stellate cell activation is regulated by fatty acids and ER stress.* Exp Cell Res, 2017. **359**(1): p. 76-85.

130. Storck, H., et al., *Ion channels in control of pancreatic stellate cell migration.* Oncotarget, 2017. **8**(1): p. 769-784.

131. Masamune, A., et al., *Differential roles of signaling pathways for proliferation and migration of rat pancreatic stellate cells.* Tohoku Journal of Experimental Medicine, 2003. **199**(2): p. 69-84.

132. Bachem, M.G., et al., *Pancreatic carcinoma cells induce fibrosis by stimulating proliferation and matrix synthesis of stellate cells.* Gastroenterology, 2005. **128**(4): p. 907-921.

133. Hwang, R.F., et al., *Cancer-associated stroma fibroblasts promote pancreatic tumor progression.* Cancer Research, 2008. **68**(3): p. 918-926.

134. Mahadevan, D. and D.D. Von Hoff, *Tumor-stroma interactions in pancreatic ductal adenocarcinoma.* Molecular Cancer Therapeutics, 2007. **6**(4): p. 1186-1197.

135. Apte, M.V. and J.S. Wilson, *Dangerous liaisons: Pancreatic stellate cells and pancreatic cancer cells.* Journal of Gastroenterology and Hepatology, 2012. **27**:

p. 69-74.

136. Jaster, R., et al., *Peroxisome proliferator-activated receptor gamma overexpression inhibits pro-fibrogenic activities of immortalised rat pancreatic stellate cells.* J Cell Mol Med, 2005. **9**(3): p. 670-82.

137. Paulo, J.A., et al., *Cross-species analysis of nicotine-induced proteomic alterations in pancreatic cells.* Proteomics, 2013. **13**(9): p. 1499-1512.

138. 田蕾, et al., *人胰腺星状细胞分离方法改良.* 南京医科大学学报（自然科学版）, 2015. **35**(5): p. 595-599.

139. Wallbaum, P., et al., *Antifibrogenic effects of vitamin D derivatives on mouse pancreatic stellate cells.* World J Gastroenterol, 2018. **24**(2): p. 170-178.

140. Omary, M.B., et al., *The pancreatic stellate cell: a star on the rise in pancreatic diseases.* Journal of Clinical Investigation, 2007. **117**(1): p. 50-59.

141. Erkan, M., et al., *The Activated Stroma Index Is a Novel and Independent Prognostic Marker in Pancreatic Ductal Adenocarcinoma.* Clinical Gastroenterology and Hepatology, 2008. **6**(10): p. 1155-1161.

142. Fu, Y., et al., *The critical roles of activated stellate cells-mediated paracrine signaling, metabolism and onco-immunology in pancreatic ductal adenocarcinoma.* Mol Cancer, 2018. **17**(1): p. 62.

143. Nagathihalli, N.S., et al., *Pancreatic stellate cell secreted IL-6 stimulates STAT3 dependent invasiveness of pancreatic intraepithelial neoplasia and cancer cells.* Oncotarget, 2016. **7**(40): p. 65982-65992.

144. Mutgan, A.C., et al., *Insulin/IGF-driven cancer cell-stroma crosstalk as a novel therapeutic target in pancreatic cancer.* Mol Cancer, 2018. **17**(1): p. 66.

IV. Acknowledgment

First, I want to show gratitude to Prof. Dr. Alexandr Bazhin from Ludwig-Maximilians-Universität München, who has provided a lot of help and offered many valuable suggestions for the improvement of my project. Prof. Dr. Alexandr Bazhin's excellent professional knowledge, rigorous logical thinking, and friendly personality have set a wonderful example for me in my future work and scientific research.

Next, I want to acknowledge my supervisor, PD Dr. med. Jan G. D'Haese, who had always given helpful help when I faced problems. From the selection of the project to the demonstration of the project, this project has been completed under his careful supervision. In addition, PD Dr. med. Jan G. D'Haese has also provided me lots of opportunities to show our results in several international conferences, which made me meet many great people in my scientific field.

In addition, I want to thank the researchers of our laboratory biobank, Maresa Demmel, Dennis Nothdurft, and Tommi Bauer, who has helped get many tissues for me and make my project go smoothly. Additionally, my colleges Chun Zhang, Zhiqiang Li, and Quan Li gave me much excellent advice and assisted me a lot in this project.

I appreciate my parents Chang Wu and Changhong Yang, my wife, Chun Zhang, who always gave me enough support and trust and encouraged me in times of frustration.

Furthermore, I wish to acknowledge Prof. Yi Miao and Prof. Kuirong Jiang from Nanjing Pancreas center, who taught me a lot during my master period and recommended me to study further in Germany. Besides, I want to acknowledge Dr. Zipeng Lu, who offered me great help in applying for study at LMU, and the China Scholarship Council, which provided funding for my studies.

Finally, I hope to express sincere gratitude to my doctor father, Prof. Dr. med. Jens Werner provided me this precious chance to conduct research in LMU. In the doctoral period, not only have I harvested a wealth of scientific knowledge and the way of scientific thinking, but also a deeper understanding of a different culture. I am also delighted and fortunate to have met so many friendly persons and visited many interesting places in the doctoral period. This extraordinary experience will make me remember forever.